Wind-Induced Loads on Roof Overhangs
Project# B83FC1

Submitted to:

Florida Building Commission

Florida Department of Business and Professional Regulation

Mo Madani, Program Manager

Building Codes and Standards 2555 North Shumard Road
Tallahassee, Florida 32399

Laboratory for Wind Engineering Research (LWER), Extreme Events Institute (EEI)

Florida International University (FIU)

Prepared by:

Project PI: Ioannis Zisis, Associate Professor, CEE, Florida International University, USA
Project Co-PI: Ted Stathopoulos, Professor, BCEE, Concordia University, Canada
Graduate Research Assistant: Karim Mostafa, CEE, Florida International University, USA

Date: June 2021

Contents

List of Figures

List of Tables

EXECUTIVE SUMMARY

The Laboratory for Wind Engineering Research (LWER) of the Extreme Events Institute (EEI) at Florida International University (FIU) was commissioned by the Florida Building Commission / Florida Department of Business and Professional Regulation to investigate the wind-induced loads on roof overhangs of low-rise residential buildings. The large-scale experimental campaign was carried out at the Wall of Wind (WOW) Research Experimental Facility. The setup comprises of two 1:10 scaled model configurations (2 ft and 6 ft inclined overhangs) of a low-rise hip roof building with roof slope 4:12. This report provides information on previous studies, describes the experimental and analytical tasks conducted and concludes on the research findings.

The research showed that the 2 ft overhang experienced higher suction coefficients at the edges compared to the 6 ft overhang. In addition, the results confirmed that, for both configurations, soffit pressure coefficients may be taken as the adjacent wall external pressure, as stated by ASCE7-16 for the case of positive pressure coefficients. On the contrary, negative pressure coefficients (i.e., suction) were not correlated well between the soffit and the wall. The length of the overhang did not seem to have a considerable effect on the positive pressure coefficient on walls and soffit. However, by carrying out correlation analysis and regression analysis between soffit pressure taps and upper wall taps, the 6 ft soffit seemed to be less correlated with the wall upper taps, than the 2 ft soffit. Area averaged pressure coefficients for overhangs and adjacent roof areas, were compared to the GCp plots in ASCE 7-16 for each specified zone. Results were within the limits of the provisions in zone 3 but exceeded those in zone 2e.

Remaining work to be completed in future phases may include different construction methods and geometries used in low-rise building stock for a more comprehensive comparison with ASCE 7-16. The different construction methods may include overhangs without soffit to assess the performance of overhangs under net Cp. In addition, buildings with gable roofs and hip roofs of different slopes should be considered.

1. Introduction

An overhang is an unenclosed continuation of the roof surface. Particularly on low-rise residential applications, overhangs may be open or covered by a soffit and may be cantilevered or supported. Most of the foundational belief about overhangs seems to suggest that overhangs extend no more than 2 ft, whereas, in Florida, overhangs are often much longer and are necessary for energy efficiency and livability in this semi-tropical climate. Overhangs in Florida can be cantilevered 6 ft or more, or supported, as on a terrace or porch, for 10 to 12 ft or more.

Low-rise buildings are greatly affected by extreme wind events. The risk of wind-induced failure is particularly increased on roofs and roof overhangs. The latter are commonly used in residential and industrial buildings for weather protection against wind, snow, rain, and sun. Roof overhangs are prone to damage because they are subjected to wind from both the upper and bottom surfaces (soffit). They are vulnerable to uplift forces that in some cases could trigger local or more severe failure on the roof. Researchers at CSTB [Centre Scientifique et Technique du Bâtiment (Center for Building Science and Technology)] suggested to limit the length of overhangs to 50 cm (20 in) especially for small slope roofs, Taher (2007). Nevertheless, in warmer and sunny climates, it is common to use extended overhangs that go beyond the 60 cm (2 ft) and even reach 1.8 m (6 ft). Extended overhangs resemble a roof extension like a canopy or a patio cover that is attached to the main structure. Recent studies showed that canopies may experience lower wind loads compared to those specified for roof overhangs on ASCE 7 (Zisis and Stathopoulos 2010, Candelario et al. 2014, Zisis et al. 2017).

ASCE 7-16 (2017) provides methods for analysis of the loads on overhangs, both for main wind force resisting systems (MWFRS) and component and cladding (C&C) loads, but the commentary does not provide any information as to the maximum length of overhang for which this analysis is valid. In section 30.9, it states that the pressure on the bottom covering of the roof overhang is the external pressure coefficient on the adjacent wall surface as implemented by Vickery (2008). This assumption was adopted more recently in the ASCE 7-16 (2017). In earlier versions of ASCE 7, for instance in ASCE 7 (2010), the overhang pressures considered the net pressure applied on these elements from simultaneous contributions from both the top and bottom surfaces of the overhang. Moreover, this may be an adequate assumption for a 2 ft overhang, but the pressure on the bottom surface of a 4ft or 6ft or 12ft overhang may not be a simple one-to-one wall-to-overhang pressure equivalent. The research that was done for canopies (ASCE 7-16 section 30.11), suggests that this may not be the case (Candelario et al. 2014, Zisis et al. 2017). Most importantly the research that led to the revised provisions of ASCE 7-16 did not consider any building model with roof overhangs.

In this project, wind tunnel testing using two large-scale models with different overhang lengths was carried out to investigate how the pressures on the wall relate to the overhang and for what distance. In addition, it was important to investigate at what point does the wall pressure cease to affect the overhang.

This report includes previous research done on this topic and identifies limitations and research gaps. The main body of the report is mostly focusing on the physical testing, including the model design, pressure tap instrumentation, test setup, and test protocols before moving to the experimental results and findings.

2. Previous studies on the effect of wind loads on roof overhangs.

Previous studies include both physical testing and numerical simulations. These studies provided information on the wind-induced loading on the upper and lower surface for the roof overhangs while considering different aspects and parameters. The effect of roof geometry; the overhang length, the interference effect of surrounding buildings on a single building with overhangs and severe wind events and performance of roof overhangs were among the studied aspects.

A comprehensive research on wind induced loads acting on low rise buildings was conducted previously. First, the effect of wind on eaves with higher slope roof (i.e., higher than 10°) was studied by Stathopoulos and Luchian (1994). Two models with roof slopes of 4:12 and 12:12 were tested with a geometric scale of 1:400. Open county exposure was considered for all tests with a velocity profile represented by a power law with exponent of 0.15. It was apparent that the model with roof slope of 4:12 resulted into higher loads especially on the upper overhang surface and near the gable end. Positive pressures were found to be higher on the upper surface of roof with slope of 12:12, as expected from the wind flow considerations. Furthermore, it was found that the lower surface of the 4:12 slope was subjected to higher pressures and suctions. Another study by Stathopoulos (1981) investigated the wind loads on perimeter eaves of low rise building and a codified chart of design pressure coefficient had been suggested and was adopted later in ASCE 7.

Similarly, Huang et al. (2018) investigated the wind pressure distribution on gable roofs with overhangs through an extensive amount of wind tunnel tests. The study considered 99 test cases with various roof pitches, height-depth ratios, and width-depth ratios. It was found that for roof pitch of 0° to 9.5°, the negative block (i.e., area averaged) pressure coefficient increased while for roof pitch larger than 9.5°, the block pressure coefficient linearly decreased. The negative block pressure coefficients on overhangs decreased from – 2.0 at the roof pitch of 0°– 10° to a positive block pressure coefficient of 0.1 at the roof pitch of 60°.

Some studies included the effect of overhang length for pressure coefficient variations and the relation with adjacent walls' pressure. One study was performed by Wiik and Hansen (1997) on two overhangs, 0.3 m and 3.4 m long, and a similar study by Ahmad and Kumar (2002) with three different overhangs, 0.5 m, 0.75 m and 1.0 m long. Wiik and Hansen (1997) found that for the gable roof the stagnation point occurred at 2/3 of the model height and then the pressure reduced towards the roof for the case of shorter overhang. While for the large roof overhang model the stagnation point occurred at the top of the wall indicating that the upper part of the wall was subjected to higher wind forces compared to the shorter overhang. Also, the shorter roof appeared to have higher Cp values near the edge compared to the large overhang roof. The effect of different overhang length and eave height aspect ratios on the wind pressures on a hip roof with pitch of 30° was investigated by Ahmad and Kumar (2002). The maximum peak pressures among the three overhangs have been found to occur at the edge corner of the 0.75 m overhang.

Furthermore, the effect of roughness surface and turbulence intensity have a recognized effect on the induced pressure coefficients on both roofs and roof overhangs. Wang et al. (2020) presented results from a field study during Typhoons Mujigae and Sarika, which was also supported by detailed wind tunnel tests on a 1:50 scaled model of the low-rise gable roof building that was used during the field measurements. Three terrain exposures were generated in the wind tunnel corresponding to three surface roughness length, zo = 0.3m, zo = 0.087m, and zo = 0.03m. It was found that as the turbulence intensity increases, the maximum magnitude of the RMS and

minimum pressure coefficients increases. The correlation coefficients of wind pressure were significantly influenced by the turbulence intensity on the front edge of the overhang and edge near the building wall, while the turbulence intensity had a little effect on the correlation coefficients on the corner of the roof overhang.

Some studies investigated the presence of a free-standing wall or the interference of other buildings on loads on overhangs. John et al. (2008) studied the effect of a free-standing wall (boundary wall) on the pressure variation on the overhang for a gable roof building with a 25° slope as shown in Figure 1. The study found that the edge of the overhang experiences severe changes in pressure values with change in the distance of the boundary wall from the parent building. It was found that the maximum value of the net positive pressure was when the free-standing wall was located at a distance 3h from the building, where h is the building height, while the overhang experienced the maximum negative net pressure without the wall. On a follow up study, John et al. (2011) examined the interference effect of boundary wall on pressure variation on the roof overhang, the roof, and the wall for a gable roof building. Overall, it was concluded that the boundary walls may significantly reduce the wind pressures on roof overhangs if the boundary wall distance is 3h and 1.5h from the building at a distance of 3h from the building after which there is practically no effect.
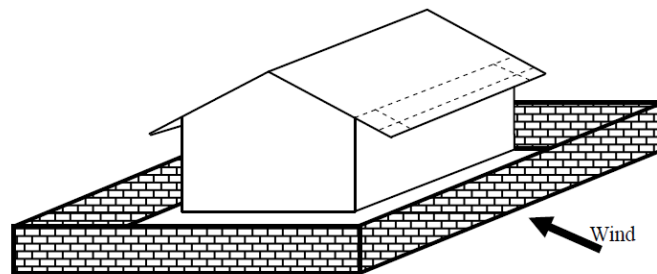
Figure 1 A sketch for a gable roof building with overhang surrounded by boundary wall
(John et al. 2008)

Major studies carried out extensive wind tunnel tests for low rise buildings with different roof types, roof slopes, eave heights, and terrain conditions but did not examine in detail the overhang loads. For instance, a comprehensive study was performed at University of Western Ontario (UWO), and the results contributed to the NIST aerodynamic database in two parts, Ho et al. (2005) and St. Pierre et al. (2005). Some pressure coefficients results, and area averaged plots were adopted into ASCE 7-16.

3. Limitations of previous studies and recommendations

The previous studies on roof overhangs included different configurations and valuable findings related to pressure coefficients on overhangs. However, some of these studies had some limitations that need to be considered and help to identify research gaps and priorities. For instance, Wiik and Hansen (1997) examined two models with two rather extreme lengths for roof overhangs (i.e., 0.3 m and 3.4 m) and did not consider intermediate lengths. Ahmad and Kumar (2002) examined three lengths of roof overhangs (i.e., 0.5 m, 0.75 m and 1.0 m) and it was found that the 0.75 m overhang had the maximum negative peak Cp while the 1.0 m overhang had the lowest value. Lengths over 1m might provide additional details on the behavior of longer overhangs.

Previous studies did not adequately examine the relation between the Cp magnitude at adjacent walls and underneath the roof overhang. Moreover, there was not enough knowledge at what overhang length does the Cp differ from the adjacent wall Cp (i.e. basic assumption implemented by Vickery (2008) and then adopted into ASCE7-16). Finally, smaller-scale models did not allow for high pressure tap resolution and did not consider any Reynolds number effects.

Therefore, in this study, physical testing at a large scale of 1:10 was conducted for two models' configurations with two different inclined overhang length (2 ft and 6 ft). The longer overhang is quite common in the State of Florida, mostly for weather-related reasons (e.g., shade, rain protection etc.), as already mentioned in this report.

4. Experimental setup and test protocol.

This section comprises the experimental test setup that was conducted at the Wall of Wind (WOW) Experimental Facility at Florida International University (FIU) (Gan Chowdhury et al. 2016). The 12-fan WOW is the largest and most powerful university research facility of its kind and can simulate a Category 5 hurricane – the highest rating on the Saffir-Simpson Hurricane Wind Scale. In 2015, the National Science Foundation (NSF) has designated the Wall of Wind as one of the nation's major "Experimental Facilities" (EF) under the Natural Hazards Engineering Research Infrastructure (NHERI) program as a distributed, multi-user national facility that provides the natural hazards research community with access to research infrastructure. The WOW EF is managed by FIU's Extreme Events Institute (EEI).

4.1.Model layouts and dimensions

Following discussions with an informal advisory group of building code officials and truss manufacturing companies, it was decided that priority should be given to the most common layouts that exist in current residential construction market. Thus, a hip roof building layout was selected, with slope 4:12, eave height of 24 ft and horizontal dimensions of 40 ft by 50 ft (full scale). To take full advantage of WOW's large experimental section, a geometric scale of 1:10 was used. The first model (Configuration A) had an inclined overhang length of 2 ft which is one of the most common lengths suggested by the truss manufacturing industry, while the other model (Configuration B) had an inclined overhang length of 6 ft which is also relatively common in the State of Florida. Models were made of polycarbonate plastic sheets and was attached to a wooden frame to eliminate vibrations. Drawings of the two configurations are shown in Figure 2 and Figure 3, respectively. Table 1 shows the scales for the different parameters in the test setup and Table 2 shows the prototype and model dimensions.
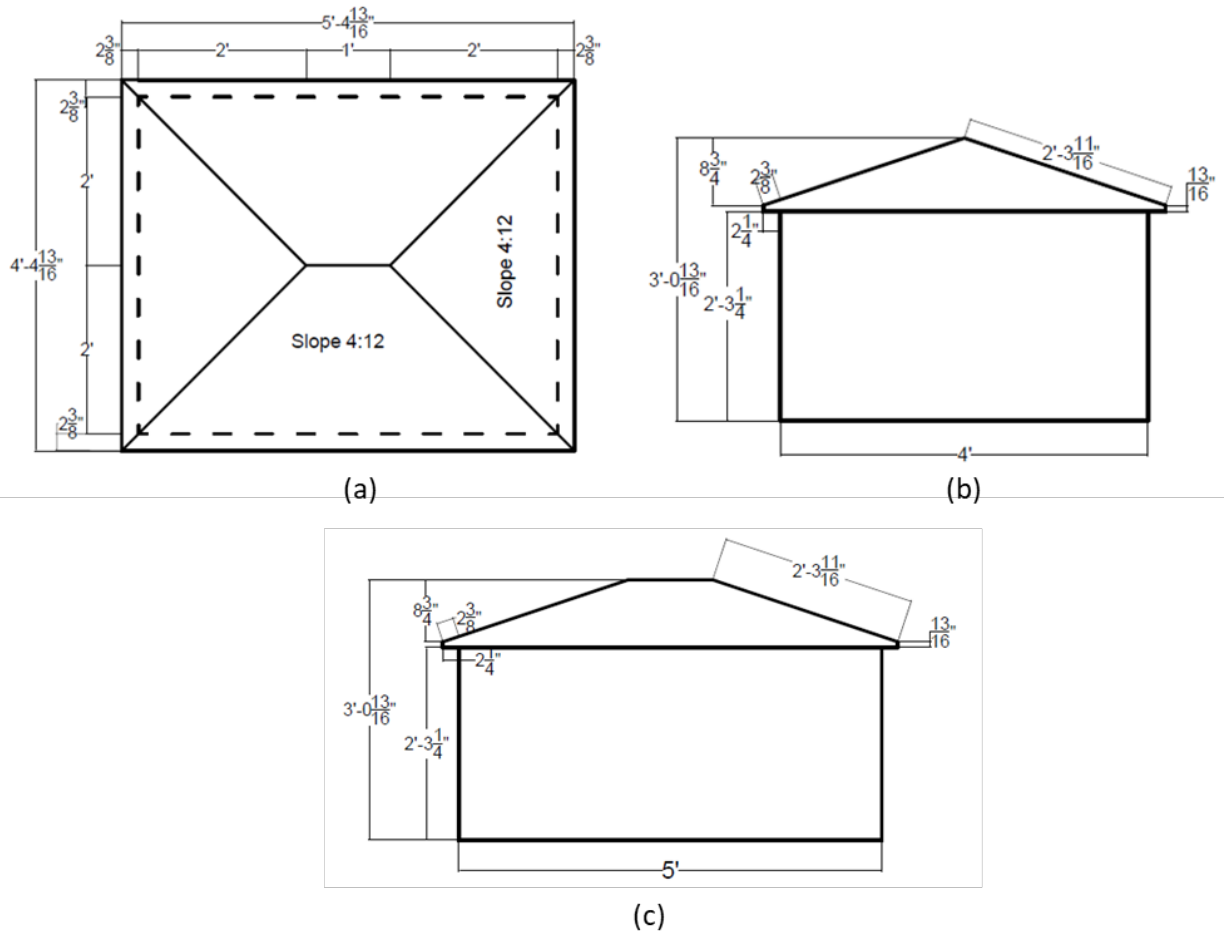
Figure 2 Configuration A model layout (a) Plan View (b) Side View (c) Elevation View (all dimensions are at model-scale)

For this set of experiments, a large length scale of 1:10 was selected to have enough space for instrumentation of pressure taps on overhangs. For instance, the 2 ft overhangs were scaled to 2.4 in, and it would have been more difficult to put the same taps on a smaller scale. Froude number and Strouhal number were preserved and kept constant between the full scale (prototype) and the scaled model. Froude number is a dimensionless number defined as the ratio between the inertial force to the external field ($F = \frac{V}{\sqrt{gL}}$, where V is the flow velocity, g is the gravitational acceleration, L is the characteristic length). Since the gravitational acceleration is the same between the prototype and the model, the velocity scale is related to the square root of the length scale. Strouhal number is a dimensionless number describing the flow mechanism oscillation ($S = \frac{FL}{V}$ where F is the vortex shedding frequency, L is the characteristic length and V is the flow velocity). Thus, the frequency scale has been related to the velocity and length scale accordingly. The time scale was calculated as the reciprocal of the frequency scale which is the same as the ratio between the length scale to the velocity scale, see table 1.
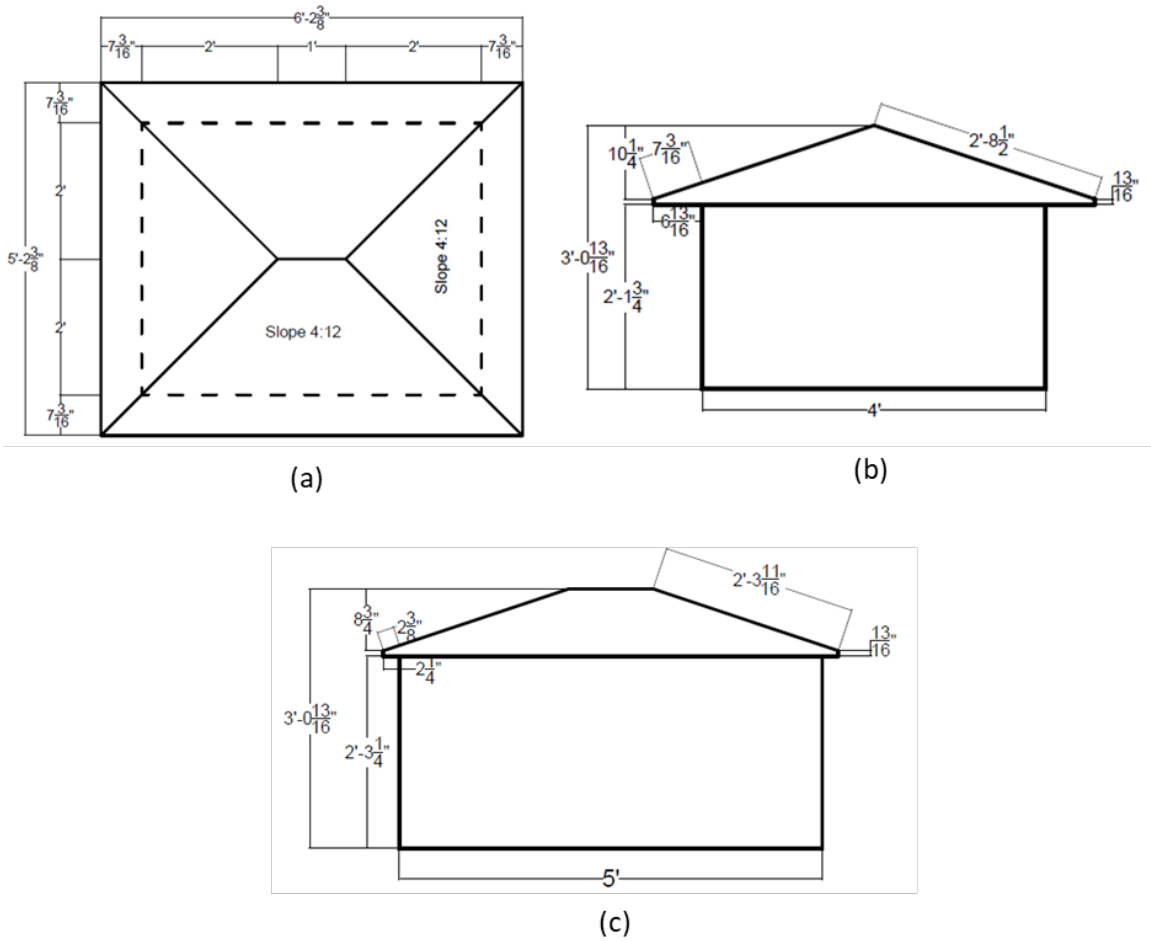
Figure 3 Configuration B model layout (a) Plan View (b) Side View (c) Elevation View (all dimensions are at model-scale)

Table 1 Testing parameters scale factors.

Parameters	Scale Factor
Length	1:10
Velocity	1:√10
Frequency	√10
Time	1:√10

Table 2 prototype and Models dimensions

| Configuration | Model | Roof Slope | Building Dimensions | | Scale | Model Dimensions | |
| | | | L x W x h | Overhang | | L x W x h | Inclined Overhang |
			(ft)	(ft)		(ft)	(in)
A	Hip Roof	4:12 (18.4°)	50 x 40 x 24	2	1:10	5 x 4 x 2.4	2.4
B	Hip Roof	4:12 (18.4°)	50 x 40 x 24	6	1:10	5 x 4 x 2.4	7.2

4.2.Instrumentation and test protocol

Pressure taps were added on the walls, the top surface of the overhangs and the bottom surface of soffits, as well as on the roof area adjacent to overhangs. The pressure taps on the roof and overhangs were placed within zone 3 and 2e as specified in ASCE 7-16. The pressure taps were connected to a sensitive pressure scanning system (Scanivalve ZOC33). The maximum pressure that could be measured by this module is 0.36 psi (51.84 psf). This pressure could be reached at about 90 mph for smooth flow, and about 60 mph for turbulent flow.

The experimental tests were conducted for 40 wind direction for each model (i.e., 0° → 360° with increments of 10 degrees plus the four corners) as shown in Figure 4 with a target wind speed of 40 mph (17.88 m/s) generated by the fans. The sampling time for each direction was 60 seconds and the sampling frequency was 520 (Hz). The two models were tested for two terrain roughness (open terrain for z_o=0.02 and suburban terrain for z_o=0.2, i.e., category 'C' and category 'B" per ASCE 7, respectively). The nominal wind speed at roof mean height varies between the two terrains because of turbulence generated from the roughness elements and spires upstream of the turntable, 22.3 m/s for open terrain and 20.9 m/s for suburban terrain. Figure 6 and Figure 8 show the two-story hip roof model tested in the WOW for both configurations.
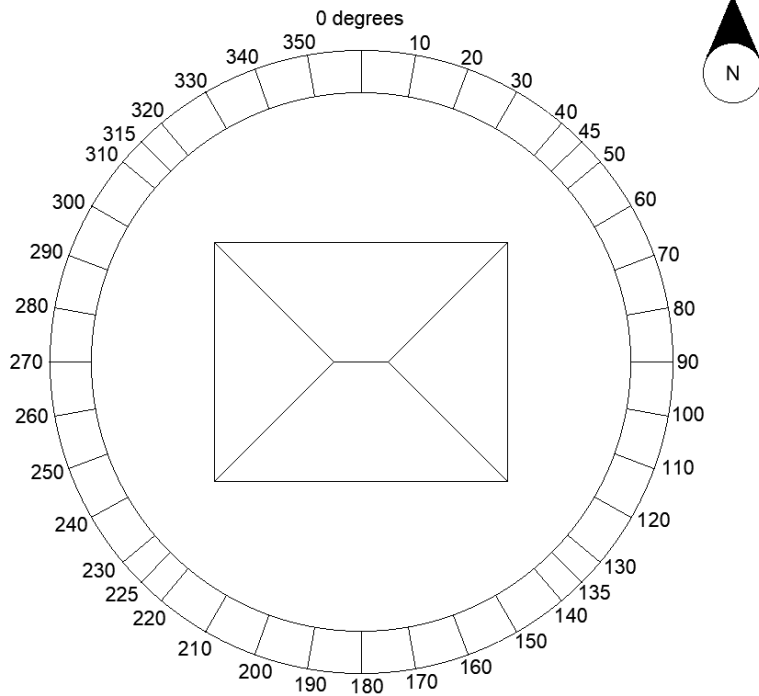
Figure 4 Wind directions tested at the wall of wind.

Table 3 Measurement configurations and parameters

Model Scale	1:10
Sampling frequency	520 H
Sampling period	60 s
Test angles	0º:10º:360º, 45º, 135º, 225º and 315º
Upstream exposures	Open and suburban
Nominal wind speed at reference height	22.3 m/s and 20.9 m/s

Configuration A had 345 pressure taps placed on walls, soffits, roof with overhangs, and configuration B had 360 pressure taps. The pressure taps were added on two sides (walls, soffit, and roof with overhangs) of each model since the models are symmetric and were tested for 360° as shown in Figure 5 and Figure 7 . The two sides, where pressure taps were added, were identified as south and east sides for data analysis as discussed later in this report. The south side corresponds to the 5 ft wall and the east side corresponds to the 4 ft wall. Pressure taps at each wall were placed with equal spacing with the adjacent soffit for correlation analysis purpose as discussed later in this report.
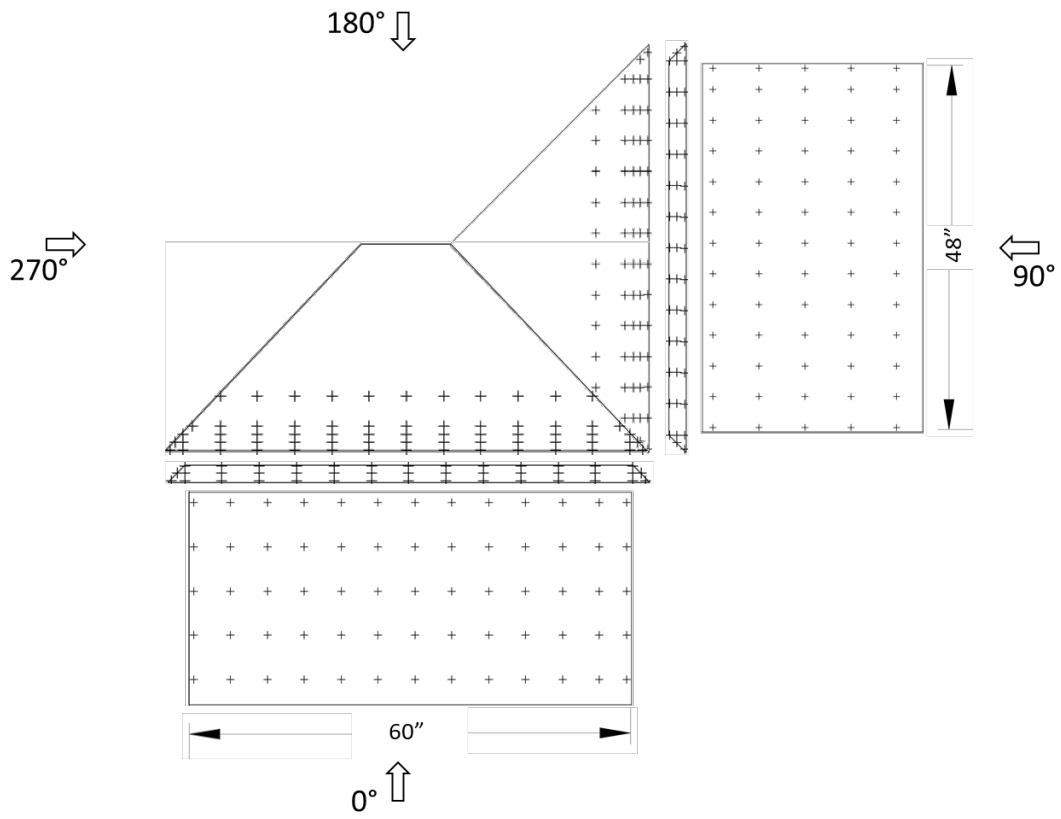
Figure 5 Pressure taps layout on configuration A on walls, soffits, and roof with overhangs.

Figure 6 Model A Configuration on the turntable at the Wall of Wind.
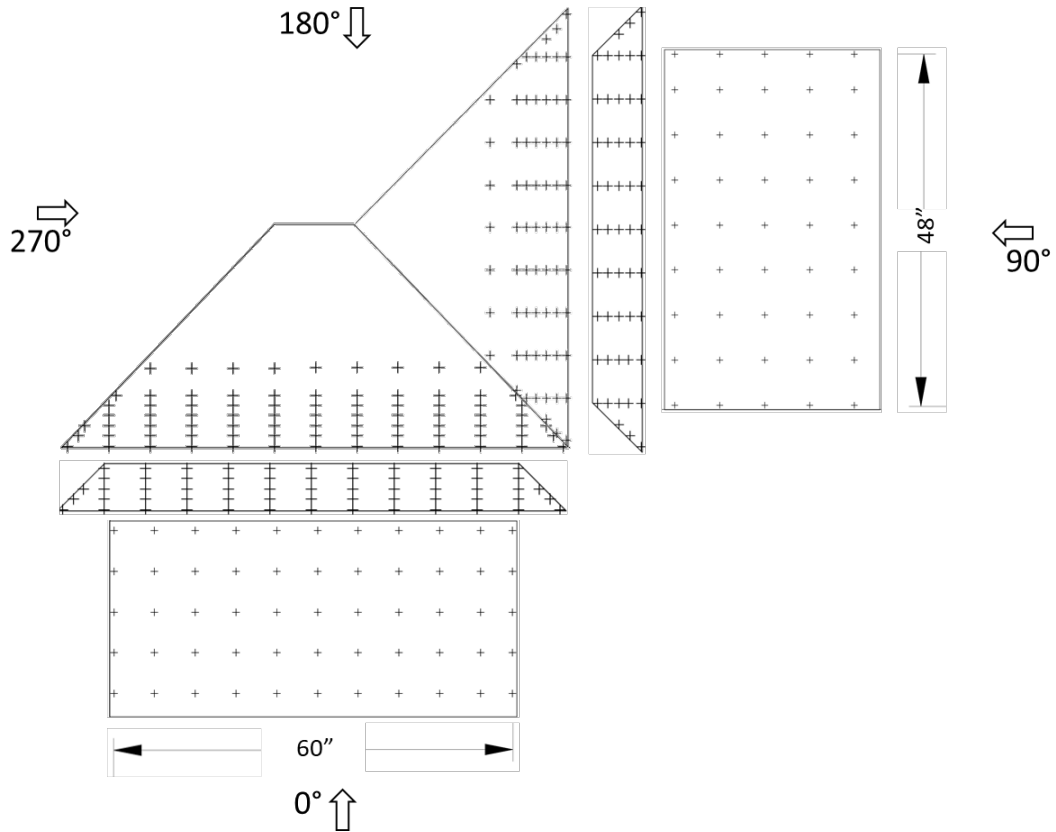
Figure 7 Pressure taps layout on configuration B on walls, soffits, and roof with overhangs.

Figure 8 Model B Configuration on the turntable at the Wall of Wind.

5. Results and discussion

Data analyses were performed on the data acquired from the conducted experimental testing. The acquired raw data for each pressure tap measure the relative pressure between the pressure at the tap location and the static pressure at the WOW in psf. First, the data went through a transfer function for correction of the tubing distortion - a onetime process done for any wind testing project

using flexible tubing to connect pressure taps to the pressure scanners. The purpose is to correct the distortional pressure data caused by the length effect of the tubing (Irwin et al. 1979). Afterwards, a post-test Partial Turbulence Simulation (PTS) was performed to account for the missing low frequency part of the spectrum (Mooneghi et al. 2016; Moravej 2018). Table 4 and Table 5 show the parameters used for PTS for open and suburban terrain, respectively.

Table 4 PTS parameters for open terrain

	Prototype		Model	
Iu% (Turbulence Intensity)	Iu_p	16.45%	Iu_m	8.11%
Lu (Length Spectrum) (m)	Lu_p	116.3	Lu_m	1.393
H (Roof height) (m)	b_p	8.763	b_m	0.8763
V (m/s)	U_p	70.51	U_m	22.3
test time (minutes)	T_p	3.162	T_m	1

Table 5 PTS parameters for suburban terrain

	Prototype		Model	
Iu% (Turbulence Intensity)	Iu_p	23.27%	Iu_m	11.50%
Lu (Length Spectrum) (m)	Lu_p	63.8	Lu_m	0.771
H (Roof height) (m)	b_p	8.763	b_m	0.8763
V (m/s)	U_p	66.09	U_m	20.9
test time (minutes)	T_p	3.162	T_m	1

5.1. Wind speed and turbulence intensity profiles.

Wind speed profile measurements have been taken for each of the terrain simulations before testing. Two terrain exposures were generated in the wind tunnel corresponding to two surface roughness length, zo=0.02m and zo=0.2m for open terrain (exposure C) and suburban terrain (exposure B), respectively. Different iterations were generated at the WOW to adjust the automated roughness element and spires angles to match ESDU wind profile. Figure 9 and Figure 12 show the wind speed and turbulence intensity profile for open terrain and suburban terrain, respectively for scale 1:10. The turbulence intensity profile did not match with the ESDU because of the missing low frequency but was compensated by the post-test PTS approach. The automatic roughness elements were at 15 degrees and spires were at 30 degrees for open terrain, and at 25 degrees and 45 degrees for suburban terrain. The wind spectra were compared with Von Karman spectrum at full scale. For suburban terrain, the wind spectrum at the roof mean height 34.5 in (0.876m) adequately matched the Von Karman at zo=0.2m. On the other hand, the wind spectrum did not match well with the recommended value of zo=0.02 but matches well at zo=0.08m (see Figure 10 and Figure 11) -note that for open terrain zo ranges from 0.01m to 0.15m according to table C26.7-1 in ASCE7-16,
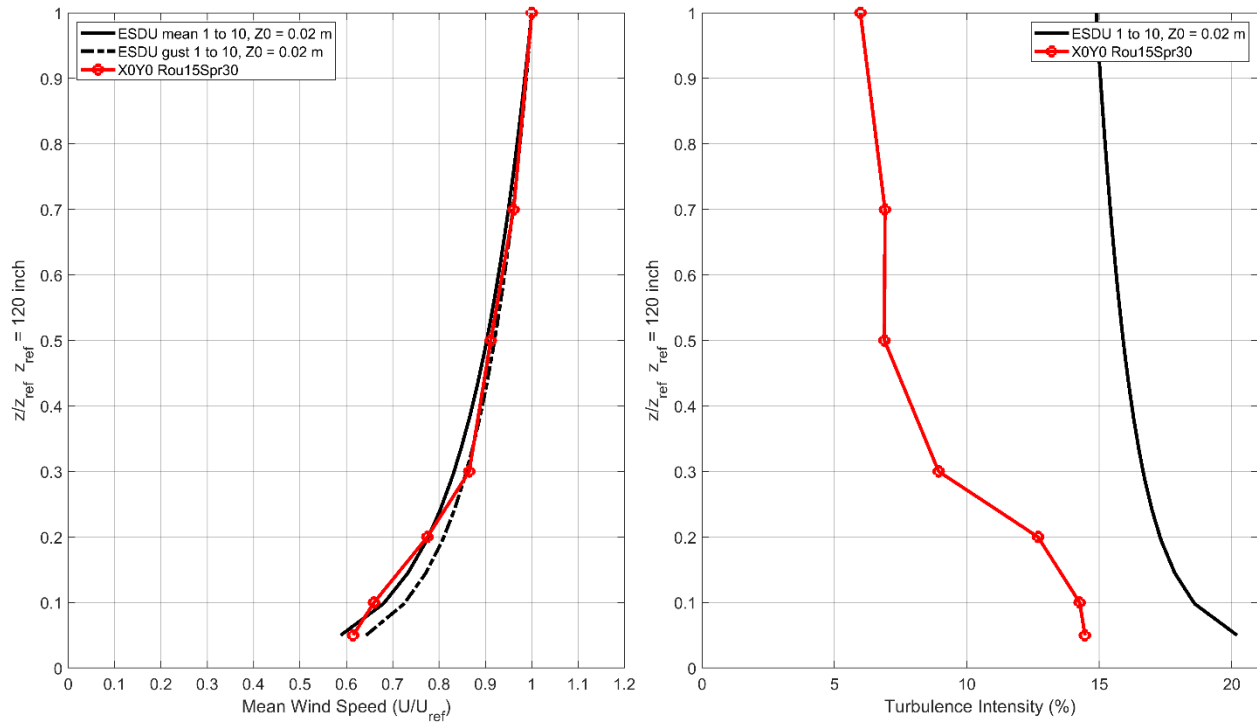
Figure 9 Wind speed and turbulence intensity profile for open terrain setup for 1:10 scale.
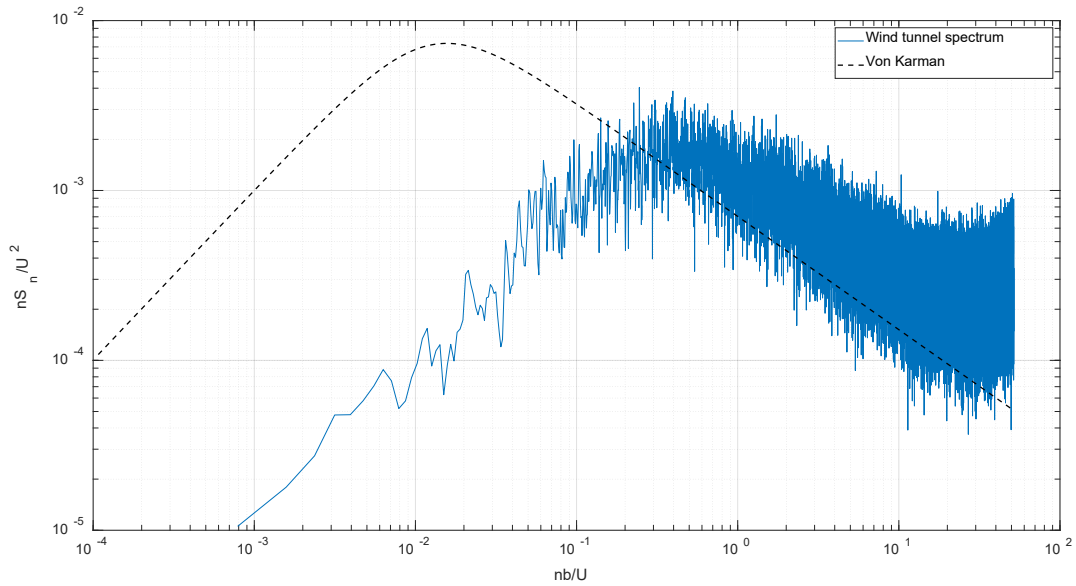
Figure 10 Wind spectra for cobra probe at roof mean height 34.5 inch for open terrain for z_o=0.02m.
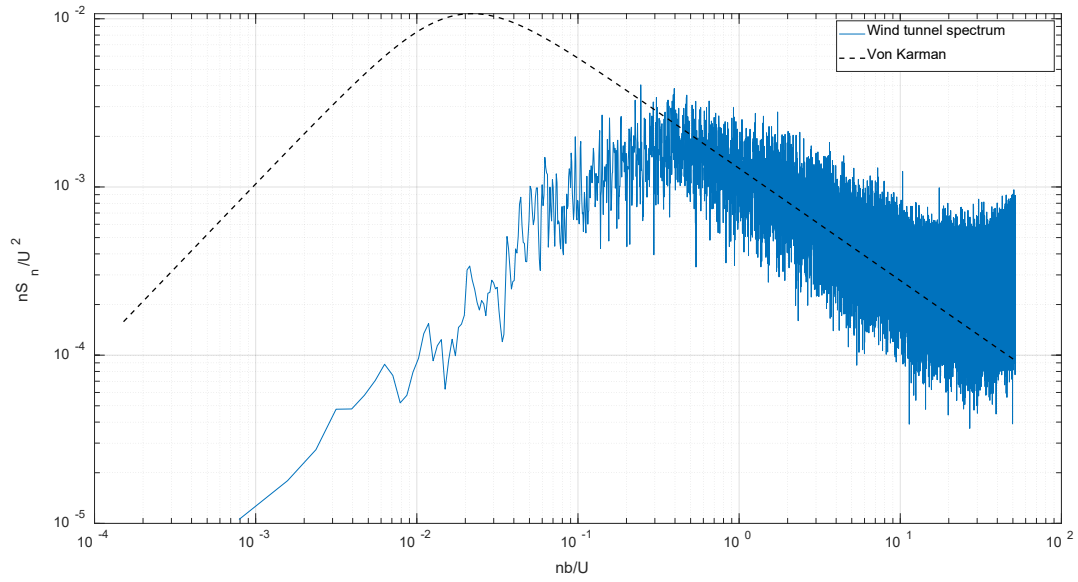
Figure 11 Wind spectra for cobra probe at roof mean height 34.5 inch for open terrain for z_o=0.08m.
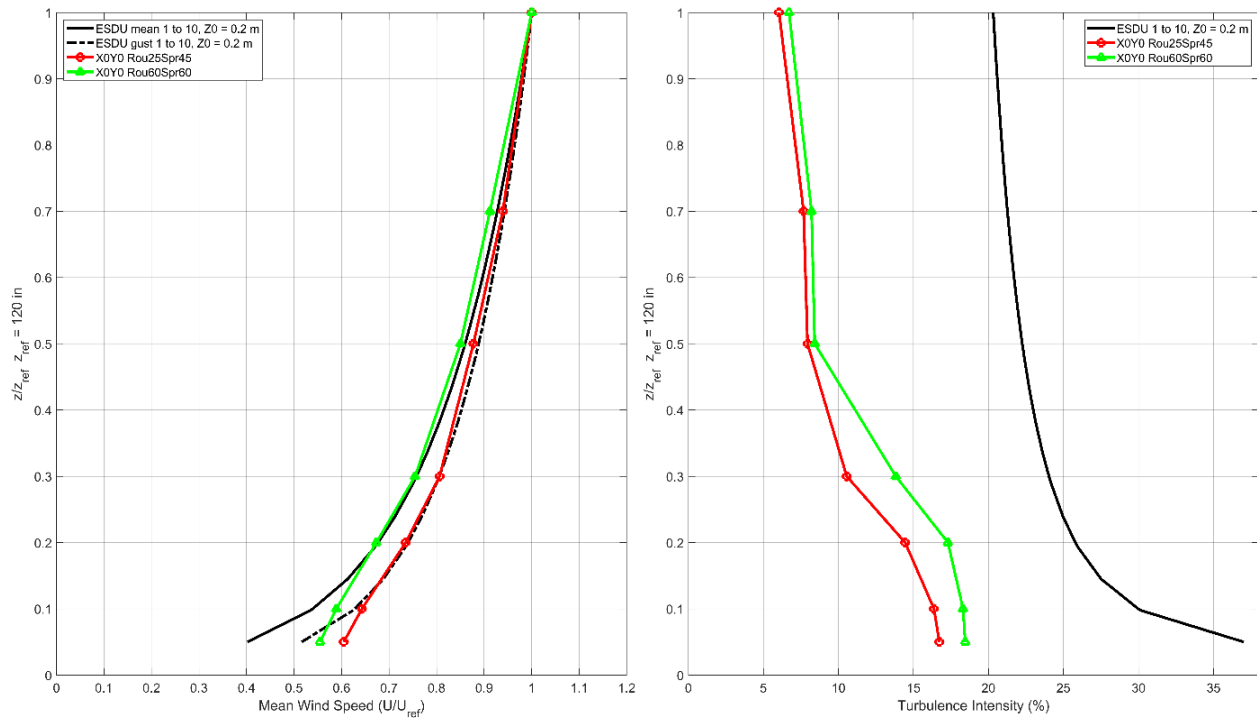
Figure 12 Wind speed and turbulence intensity profile for suburban terrain setup for 1:10 scale.
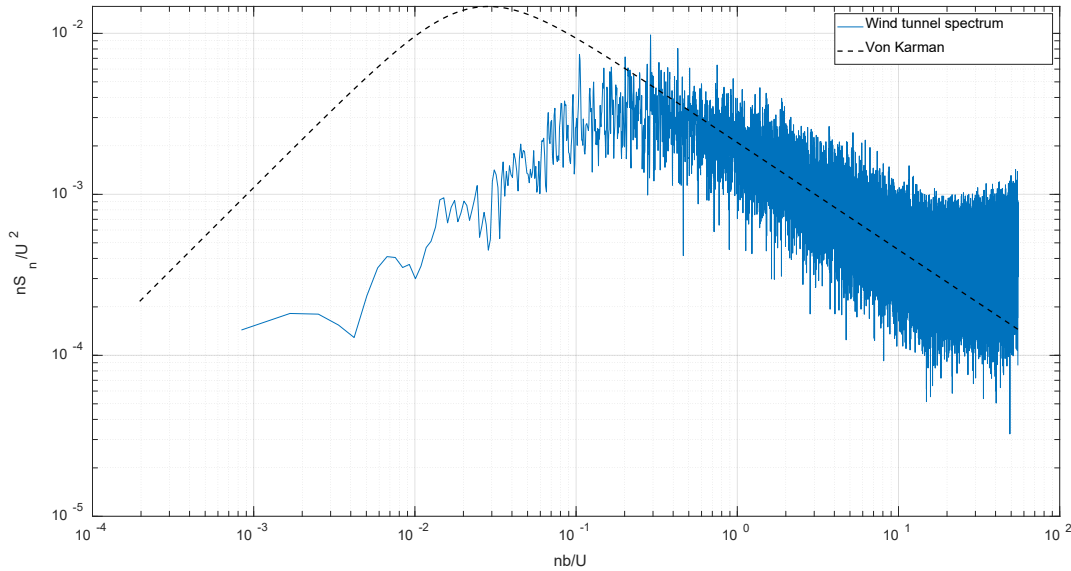
Figure 13 Wind spectra for cobra probe at roof mean height 34.5 inch for suburban terrain for z_o=0.2m.

5.2. Pressure Results

As mentioned earlier, the pressure scanning modules used in the aerodynamic test measure the relative pressure in psf. These pressure values are presented here as normalized pressure coefficients (Cp) computed using equation 1, where ΔP is the relative pressured at the tap location, ρ is the air density $1.225\ kg/m^3$, V_{ref} corresponds to the mean wind speed at mean roof height (34.5in). Consequently, statistical pressure coefficient parameters were also computed by using their corresponding pressure change parameters, as shown in equation 2 and 3. Peak pressure coefficients are referred to the minimum (highest suction/negative pressure) and maximum (highest positive pressure). In a partial turbulence simulation, the testing sample time (60 sec) was divided into subintervals of sufficient duration that peak value occur in them. The peak pressure is calculated as a function of the peak pressure coefficient occurred during the subinterval, the resultant wind speed for that subinterval and flow density (Moravej et al. 2019). The resultant wind speed composed of the mean velocity over the subinterval and each of the low frequency turbulent velocity component, u_L, u_V, u_W. The partial turbulence simulation method uses Fisher Tippet Type 1 distribution in estimating the probability of the peak pressure coefficient for not exceeding that peak pressure coefficient in the subinterval. The peak pressure coefficient for each interval is calculated based on the peak pressure and the mean velocity of the full sample period with full spectrum turbulence and it is based on mean hourly dynamic pressure. The peak pressure coefficient for 3 sec is obtained by rescaling using equation 4 which is based on 3-second dust dynamic pressure. Importantly, note that for any positive sign represents a pressure directed towards the surface while a negative sign represents a pressure directed away from surface (suction). Throughout this report, peak pressure coefficients were identified either as local (single tap) or area-averaged (two or more taps).

$$Cp = \frac{\Delta P}{0.5\,\rho\,V_{ref}{}^2} \tag{1}$$

$$C_{p\;mean} = \frac{P_{mean}}{0.5\rho V_H^2} \tag{2}$$

$$C_{p\;peak} = \frac{P_{peak}}{0.5\rho V^2} \tag{3}$$

$$C_{peak\;3-sec} = Cp_{peak}\left(\frac{U}{U_{3-sec}}\right)^2 \tag{4}$$

In total, 40 wind directions were tested to determine the peak max and min Cp for each pressure tap. For any pressure tap, the time history comprises of min, max and mean Cp at any wind direction. Specifically, some wind directions were more critical than the other, even at the same wind direction the critical absolute pressure might be a result of either a positive or a negative peak. For instance, at the south side at a wind direction of 180˚, the wall and the soffit were exposed predominantly to positive pressure while the roof and the overhang were exposed to suction. Sample Cp contour plots are shown in Figure 14 to Figure 16 for the south side of model A for both open and suburban terrain and contour plots for model B are shown in Figure 17 to Figure 19. Detailed presentation of some other cases is included in Appendix A.

For model A, the peak min Cp near the overhang corner was -3.2 for open terrain and -3.25 for suburban terrain. For model B, the peak min Cp near the overhang corner is -2.45 for open terrain and -2.50 for suburban terrain. It is apparent that the terrain change did not cause a considerable effect on the roof peak suction. In addition, it was found that the 2 ft overhang was exposed to higher peak min Cp near the edge compared to the 6 ft overhang for both terrains. This was attributed to the high velocity in the z-direction at the edge, due to the walls that lead part of the flow over the roof (Wiik and Hansen 1997).
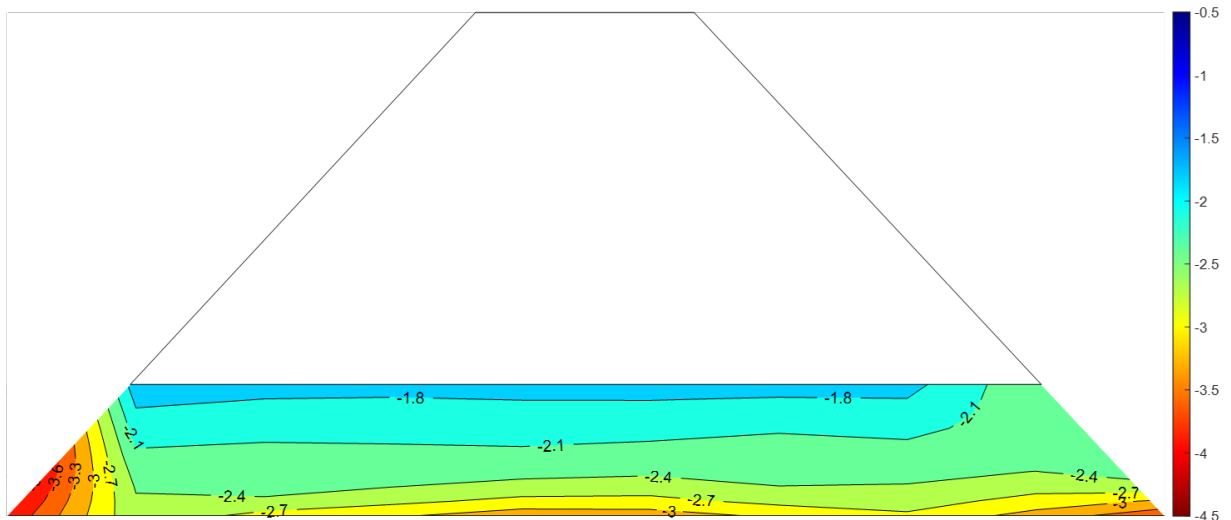
(a)
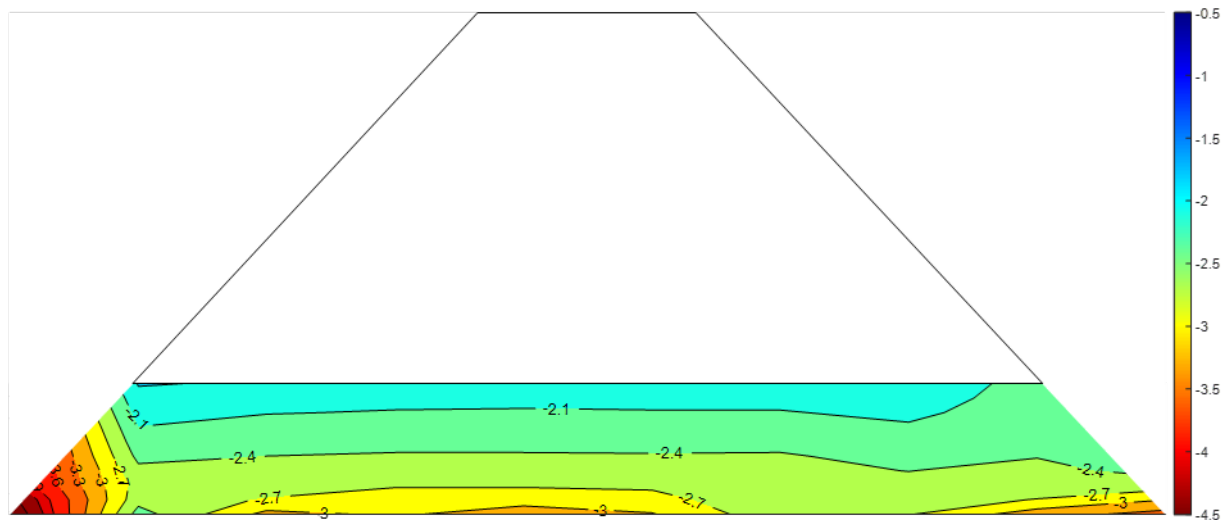
(b)

Figure 14 Peak Min for south roof of Model A at wind direction of 180º- (a) Open Terrain (b) Suburban Terrain

(a)

(b)

Figure 15 Peak Max Cp for South soffit of Model A at wind direction of 180º (a) Open (b) Suburban Terrain
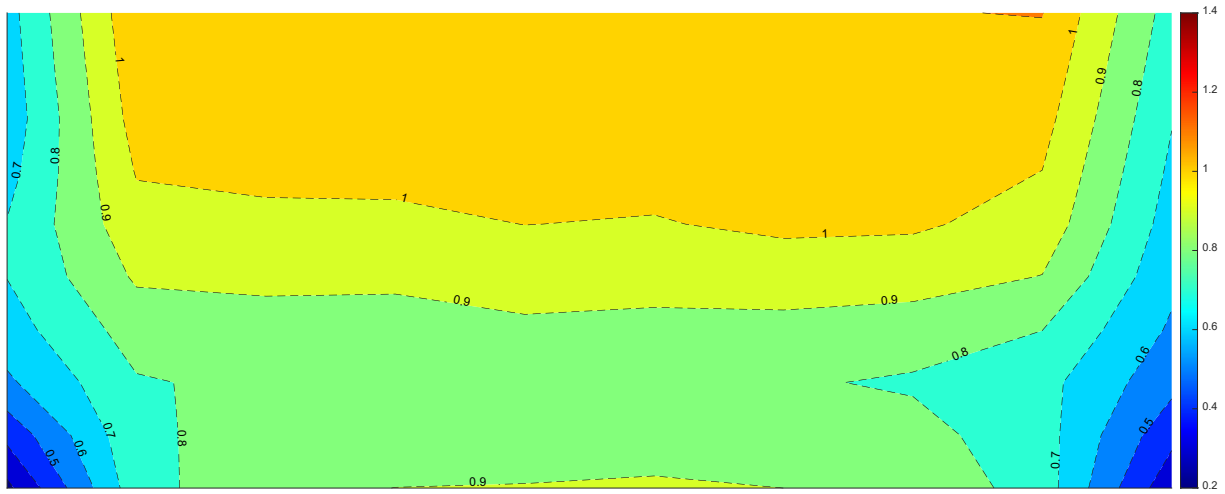
(a)
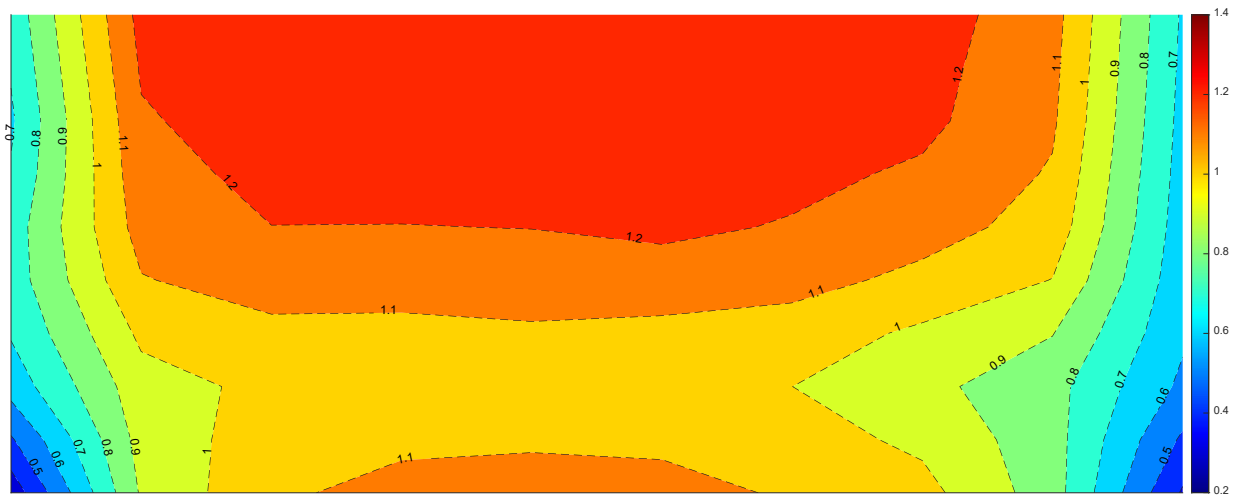
(b)

Figure 16 Peak Max Cp for South Wall of Model A at wind direction of 180º (a) Open (b) Suburban Terrain
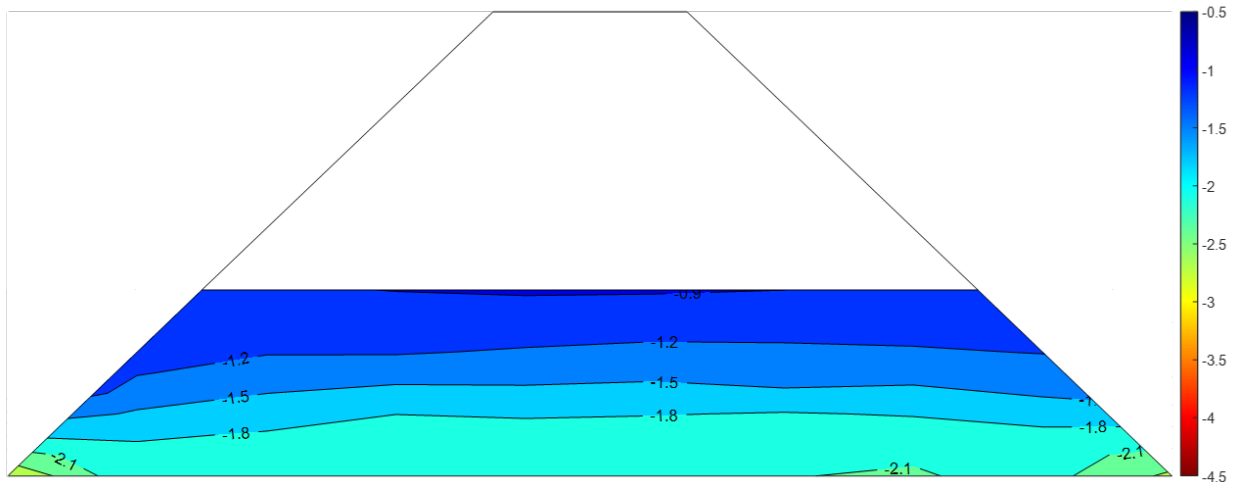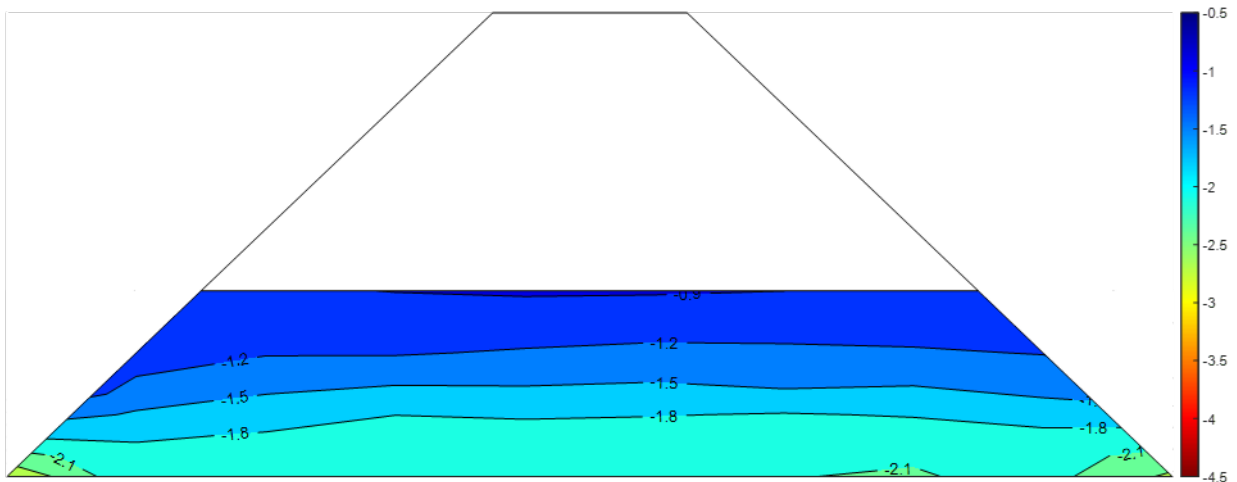
Figure 17 Peak Min Cp for South roof of Model B at wind direction of 180º (a) Open Terrain (b) Suburban Terrain

Figure 18 Peak Max Cp for South soffit of Model B at wind direction of 180º (a) Open (b) Suburban Terrain
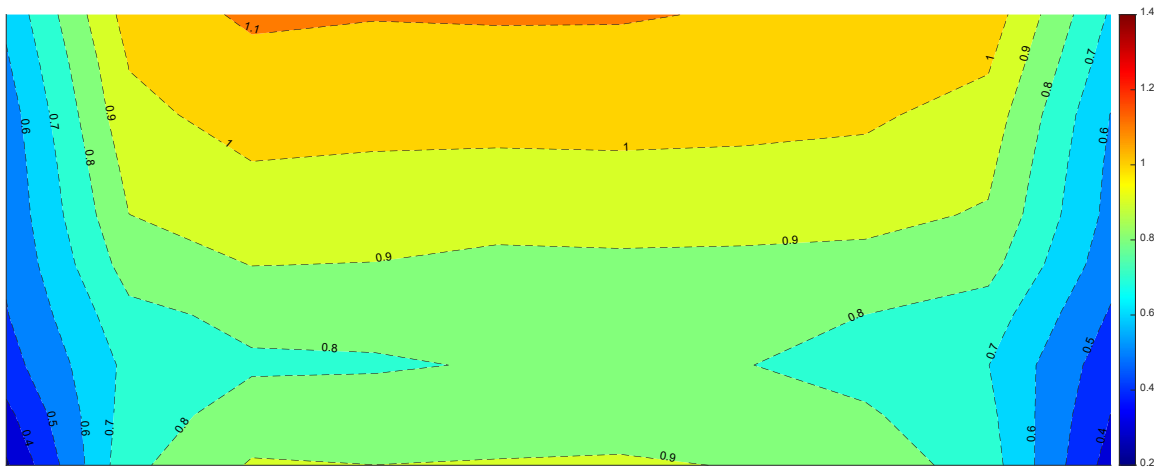
(a)
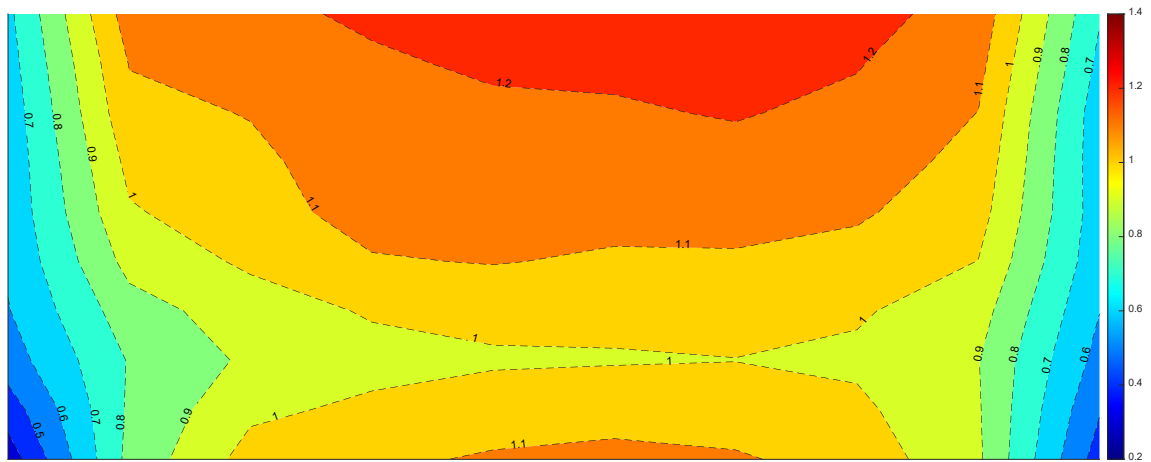
(b)

Figure 19 Peak Max Cp for South Wall of Model B at wind direction of 180º (a) Open (b) Suburban Terrain

The change of terrains caused more considerable effect on the walls and soffit compared to the roof and overhangs. Figure 20 and Figure 22 show the location of upper taps in the wall for model A and model B, respectively used in analyses. The Peak max Cp were higher in suburban terrain, this match the finding of (Kozmar 2021), where peak Cp increases as the incoming turbulence intensity increase. One of the reasons attributed to this observation is the flow in suburban terrain become more turbulent, the effect of turbulence cause the flow velocity to decrease, and accordingly the Cp increases (see Figure 21 for model A and Figure 23 model B). In Figure 21 and Figure 23, the peak Cp at the edge of the wall were not exactly symmetric, and the difference between these Cp range from 5% to 10%. Saathoff and Melbourne (1997) related the increased levels of pressure fluctuations to the shear layer vortices being in closer vicinity to the surface. Separation occurs at the sharp-edged corners of the wall, due to the existence of large pressure gradients near these locations (Milne et al. 2013). Thus, the taps at the edge have lower positive Cp compared to the adjacent taps for this wind direction. This indicates that the roughness surfaces and turbulence intensity have a minimal effect on the induced pressure coefficients on both roofs and roof overhangs, and a recognized effect on pressure coefficients on walls.

19
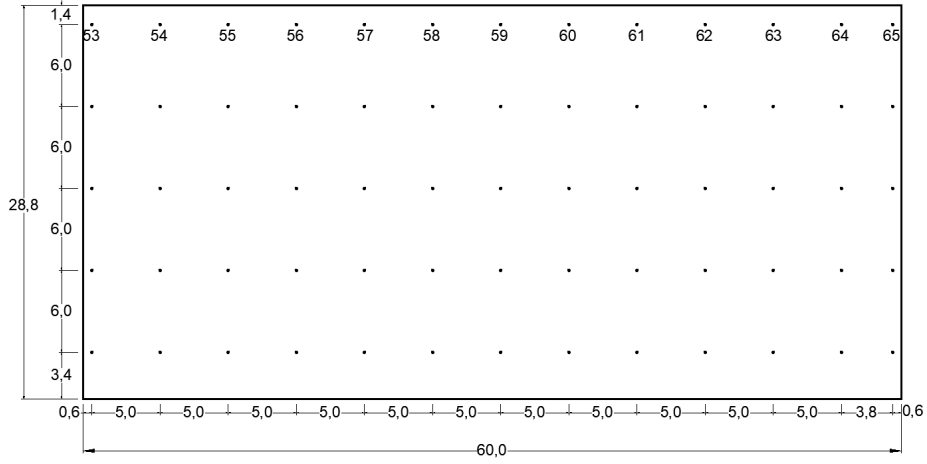
Figure 20 Location of pressure taps on Model A South Wall.
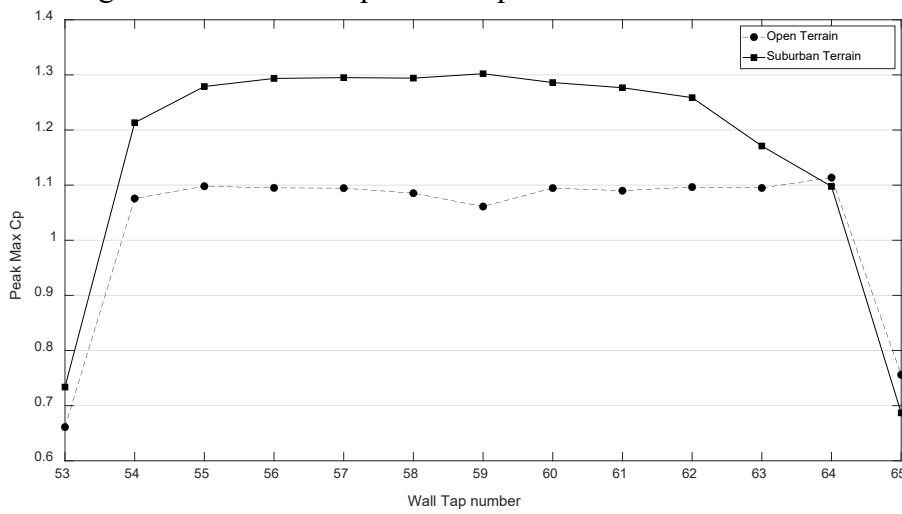
Figure 21 Effect of Roughness terrain on Max Cp for Model A Wall for wind direction of 180˚.
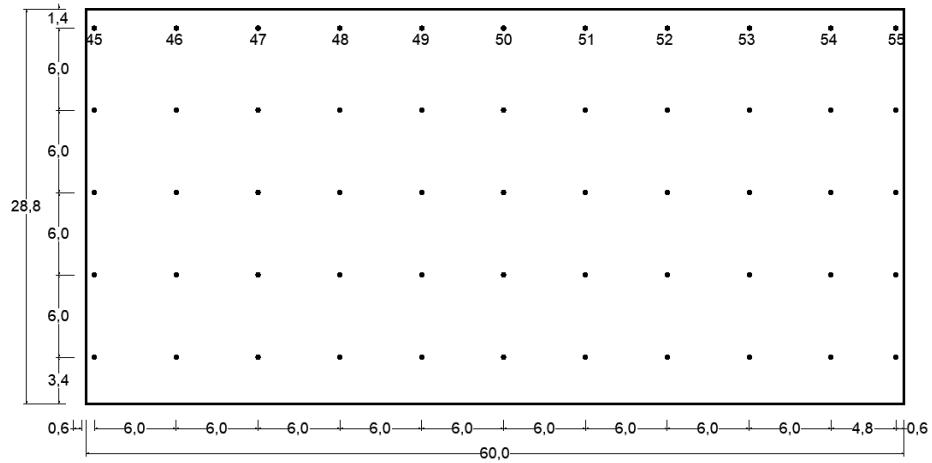
Figure 22 Location of pressure taps on Model B South Wall.
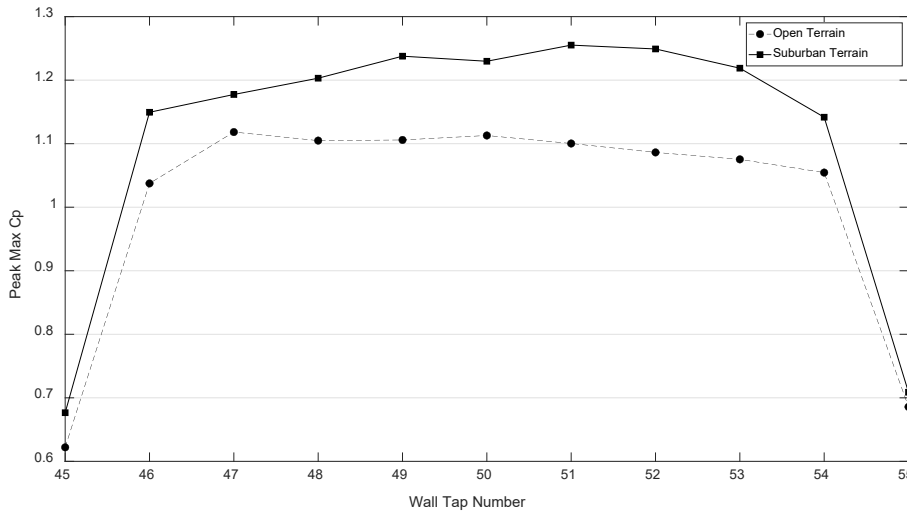
Figure 23 Effect of Roughness terrain on Max Cp for Model B Wall for wind direction of 180˚

5.3. Correlation of Soffits and Adjacent Walls

The pressure taps in the walls and soffits were placed with equal spacing, to compare the Cp of upper taps in the wall with the adjacent taps in the soffit using correlation and regression analysis. For all the figures that include the wall and the soffit, the shorter side of the soffit is the wall side (upper side), and the longer side of the soffit is the edge side (lower side). The taps in the black dashed box used as sample for middle taps correlation, while the taps in the red box used to derive the correlation coefficients and perform the regression analysis. For model A, the upper taps of the wall were compared to the three rows of taps placed in the soffit as shown in Figure 24. Likewise, for model B, the upper taps of the wall were compared with five rows of taps placed in the soffit as shown in Figure 25.
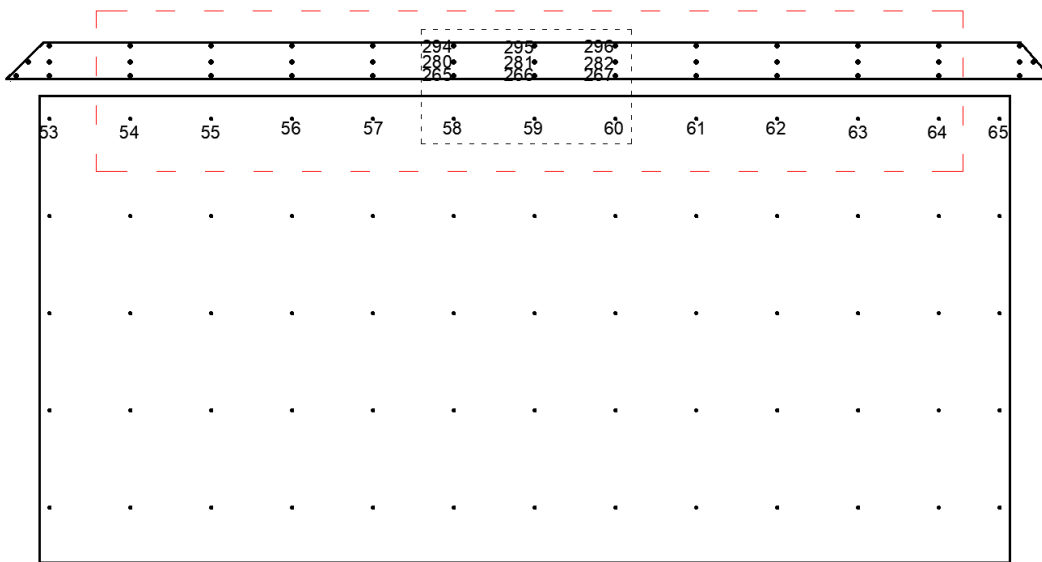
Figure 24 Location of upper taps in walls and taps in soffit used in correlation for Model A
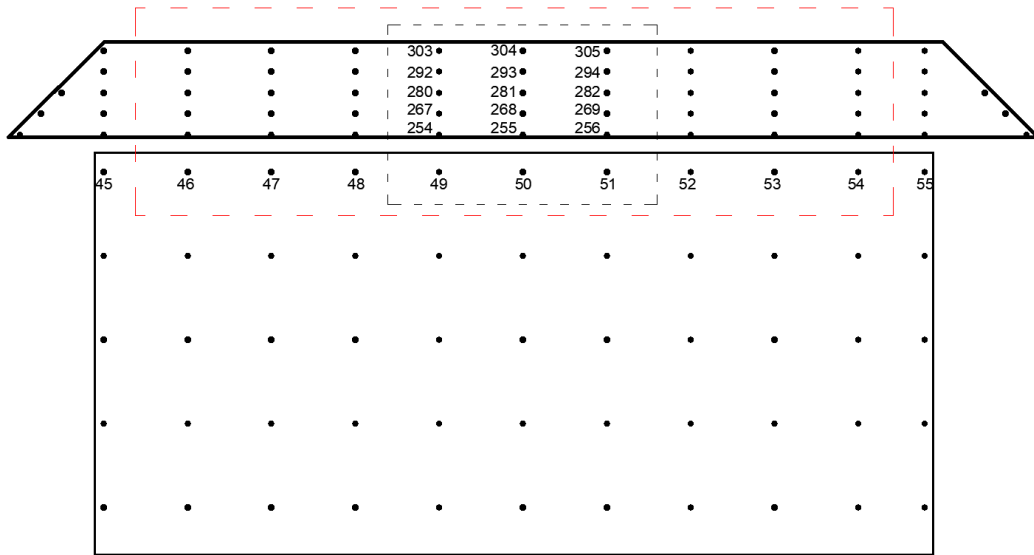
Figure 25 Location of upper taps in walls and taps in soffit used in correlation for Model B.

5.3.1 Middle Taps correlation

The three middle taps in the wall were used to display the similarity in pressure fluctuations between the upper taps of the wall with the corresponding taps in the soffit. For model A (case 1), the peak max and peak min pressure coefficients of the three upper middle taps in south wall (taps 58,59 and 60) were compared with the adjacent soffit taps for the 40 wind directions. Figure 26 displays the peak max and peak min for the chosen wall and soffit taps for all wind directions. It is apparent that the peak max Cp were very similar along the adjacent taps in all wind directions. In contrast, the peak min Cps used to slightly change for soffit taps located away from the wall. For instance, for wind directions from 135º to 225º, the wall and soffit taps were mainly exposed to positive pressure, thus, the peak min Cp ranged from 0 to -0.5, while the positive Cps values were very similar around 1. This supports the assumption in ASCE7-16 that the pressure coefficient at the bottom covering of the roof overhang shall be taken as the external pressure coefficient on the adjacent wall surface. The edge pressure taps in the soffit experienced more suction compared to the middle or the inner row. The soffit exposed to more turbulence underneath and this turbulence increased near the edge where more separation occurs. Consequently, pressure taps at the soffit edge had higher peak min Cp than the middle and inner taps.
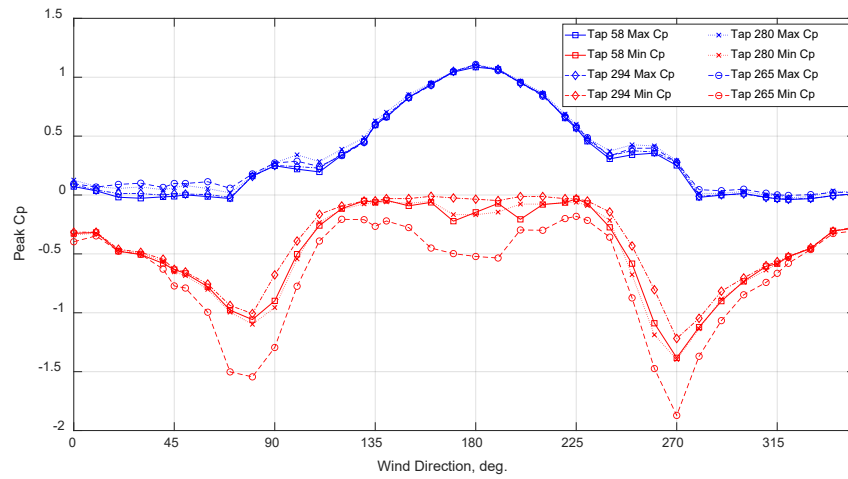
(a)
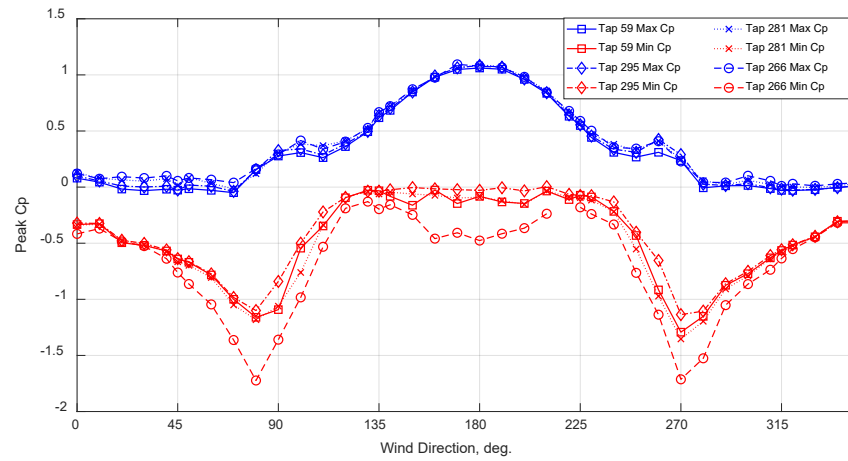
(b)
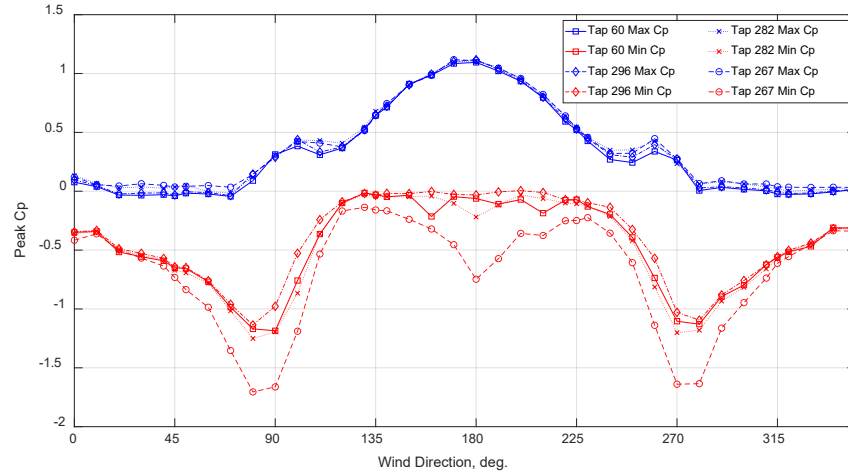
(c)

Figure 26 Peak Max and Peak Min for (a) Tap 58 (b) Tap 59 (c) Tap 60 of Model A south wall and their adjacent taps in soffits.

Similarly, for model B, the peak max and peak min pressure coefficient of the three upper middle taps in south wall (taps 49,50 and 51) were compared with the adjacent soffit taps for the 40 wind directions as shown in Figure 25. Likewise, the peak max Cps were very similar along the adjacent taps in all wind directions, while the peak min differs as the taps locate away from the wall. The taps located at the soffit's edge (i.e., away from the wall) had the highest peak min Cp. Tap 50 is the middle tap that located near to the wall center; thus, the peak Cps look symmetric along the wind directions (Figure 27a). Taps 49 and 51 located before and after the middle tap, respectively, and it is apparent from Figure 27b and Figure 27c that the Cp are mirroring at wind direction of 90°and 270°.

(a)

(b)

24
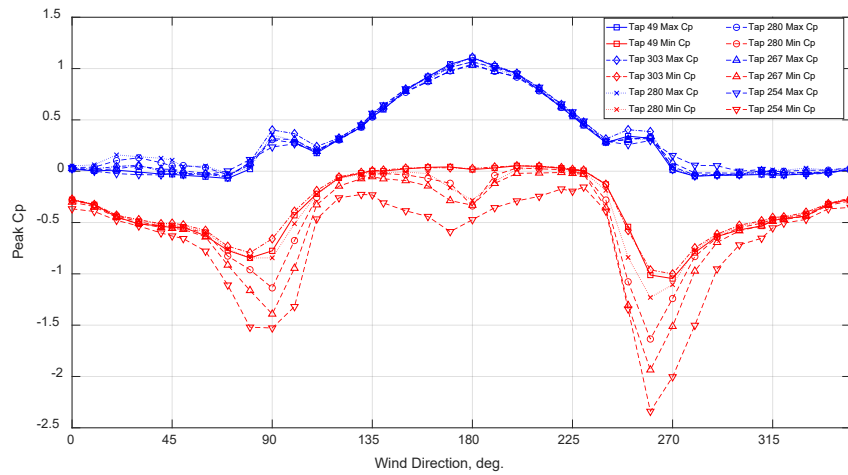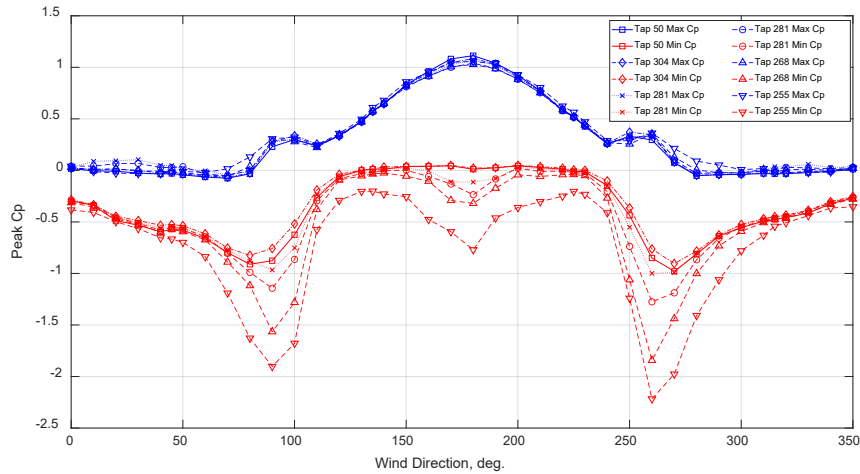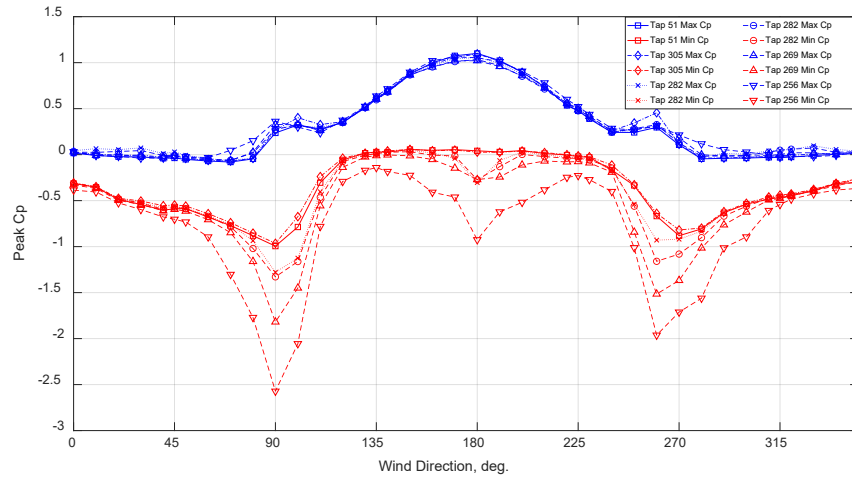
(c)

Figure 27 Peak Max and Peak Min for (a) Tap 49 (b) Tap 50 (c) Tap 51 of Model B south wall and their adjacent taps in soffits.

5.3.2 Regression Analysis and Correlation Coefficients

One of the objectives of this research study, was to correlate the effect of wall pressure to the soffit pressure and investigate how the length of soffit would affect this correlation. The three middle upper taps in the walls for both models that used before in displaying the peak max and min Cp were used to display their correlation coefficient. Correlation coefficients are used to measure the relation between two variables and one of the most common forms is the Pearson's correlation (R factor) which ranges from 0 (no correlation) to 1/-1 (perfect correlation). This factor follows equation (4) and was used later in Regression analysis as well.

$$R = \frac{\Sigma(x_i - \bar{x})(y_i - \bar{y})}{\sqrt{\Sigma(x_i - \bar{x})^2 \Sigma(y_i - \bar{y})^2}} \tag{4}$$

Figure 28 displays the correlation coefficient between the previously mentioned taps in the wall and the adjacent taps in the soffit for model A. Generally, wall taps are well correlated with soffit taps. The R factor ranges from 0.80 to 0.98 for the first row, the nearest to the wall, 0.73 to 0.97 for row two, which is the middle row, and 0.57 to 0.92 for row three, the farthest to the wall. The highest correlation occurred when the south wall and the adjacent soffit were at the windward (wind direction 180°) or in the wake region (wind direction 0°), i.e., the wall and the soffit were exposed to predominantly positive pressure or predominantly suction, respectively. Some wind directions minimize the correlation coefficients as flow separation occur along the wall and the soffit length. For instance, at wind direction 120° and 250°, suction occurred at the south and separations caused more turbulence underneath the soffit that cause reduction in correlation coefficients. It was concluded that the soffit pressure is less correlated with the wall at the edges compared to the near wall surfaces.

25
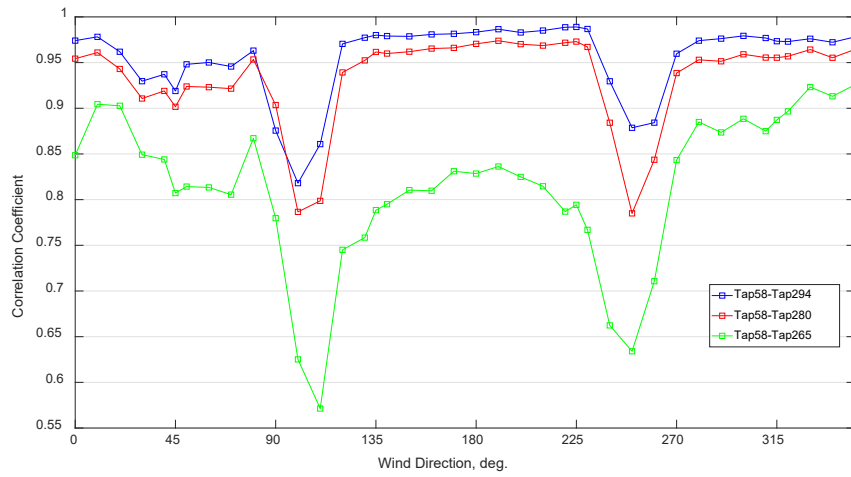
(a)
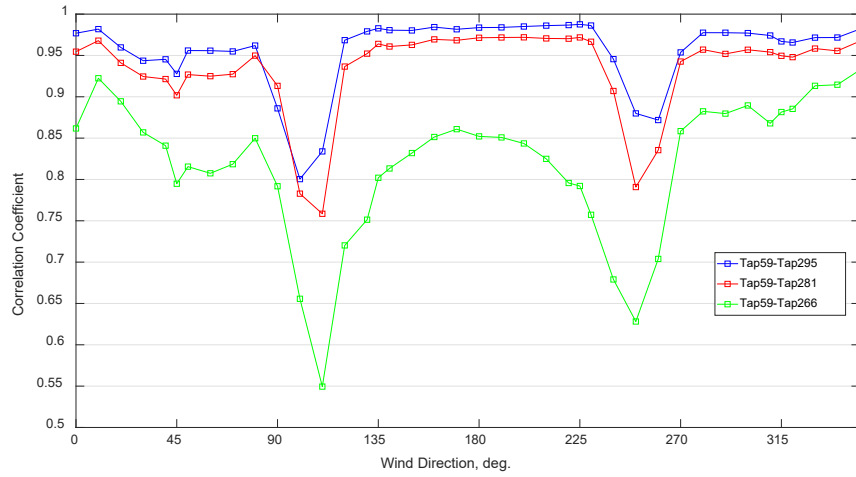
(b)
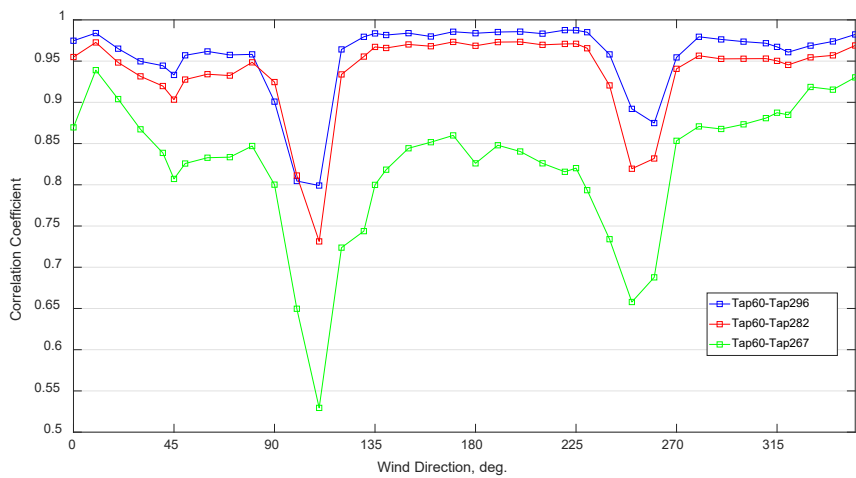
(c)

Figure 28 Correlation Coefficients between upper taps in wall (a) Tap 58 (b) Tap 59 (c) Tap 60 with adjacent taps in soffit.

26

Regression analysis was done on the wall upper taps and soffit taps for model A and B. Regression analysis was done for getting the relationship between the pressure coefficients of the soffit taps with the wall taps. This relationship either shows a decrease or increase of the pressure coefficient for each row of the soffits compared to pressure coefficients of the walls. For both models, the corner taps for walls and soffit were not considered in correlation as shown in Figure 24 and Figure 25, only the taps inside the red dashed box included in correlation, because the separation of the flow occurs at the corner of the building, so the Cp of these taps have lower Cp compared to other taps and may not be significant to be correlated together. The regression analysis compared the peak max Cp for upper wall taps with the three rows of taps in the soffit for two wind direction, 180º (normal to south wall) and 90º (normal to east wall). More precisely, each Cp value for wall taps correspond to three values for the three rows of the soffit taps. The first row is the one next to the wall and the third row is the outer edge row, similarly for model B, the first row is the adjacent to the walls and the fifth row is the edge row. The positive peak pressures were well correlated for the three rows, while for the negative peak pressure, R-squared value slightly decrease as the taps locate far from the wall. It is apparent from the regression line slope as shown in Figure 29 to Figure 31 that the soffit pressure taps have slightly higher Cp values than the wall taps, and it is a directly proportional relation. Moreover, the slope for the three lines in both directions is close to 1 and this supports the assumption in ASCE7-16 as well for positive peak pressure, however, for negative peak pressure the soffit and wall taps are not well correlated. The regression analyses match well with (Vickery 2008) for positive pressure coefficients, and negative pressure as shown in Figure 32. Vickery investigated a soffit with length of 1.67 ft (0.51m) which is corresponding to the first two rows of soffit taps for model A. Therefore, by comparing Figure 29 and Figure 30 with Figure 32, the regression and correlation analysis look very similar, while convergence in results started to happen in row 3 which is at the edge of 2 ft soffit and this is more pronounced with longer overhangs (6 ft) as will discussed later.
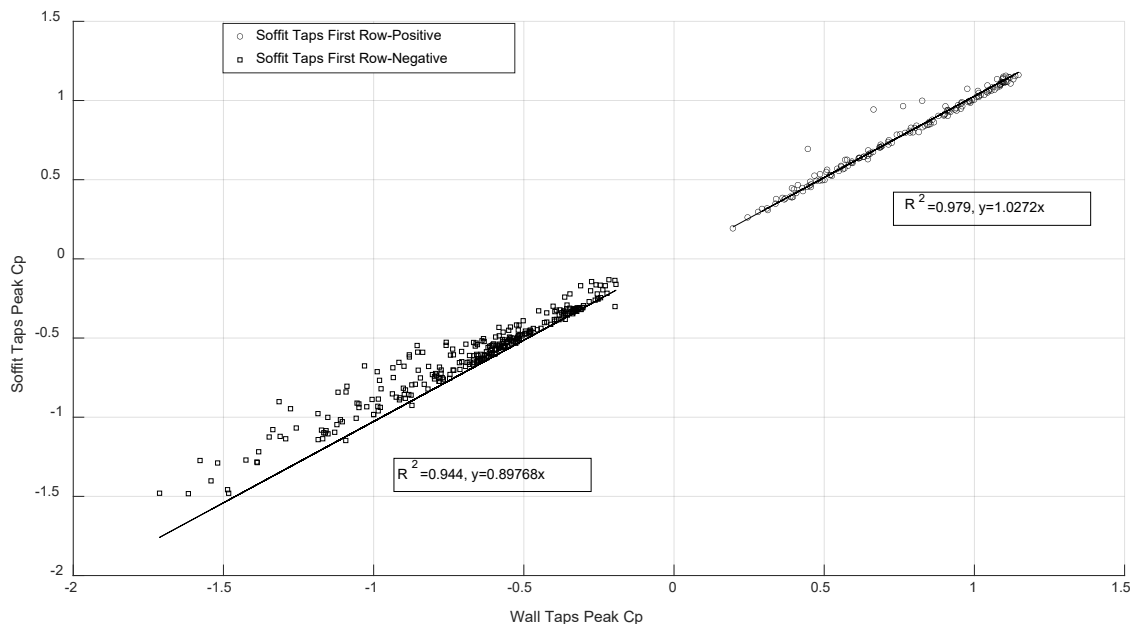
Figure 29 Linear Regression Relation between Upper Taps in South Wall and first row of taps in soffit for Model 'A'
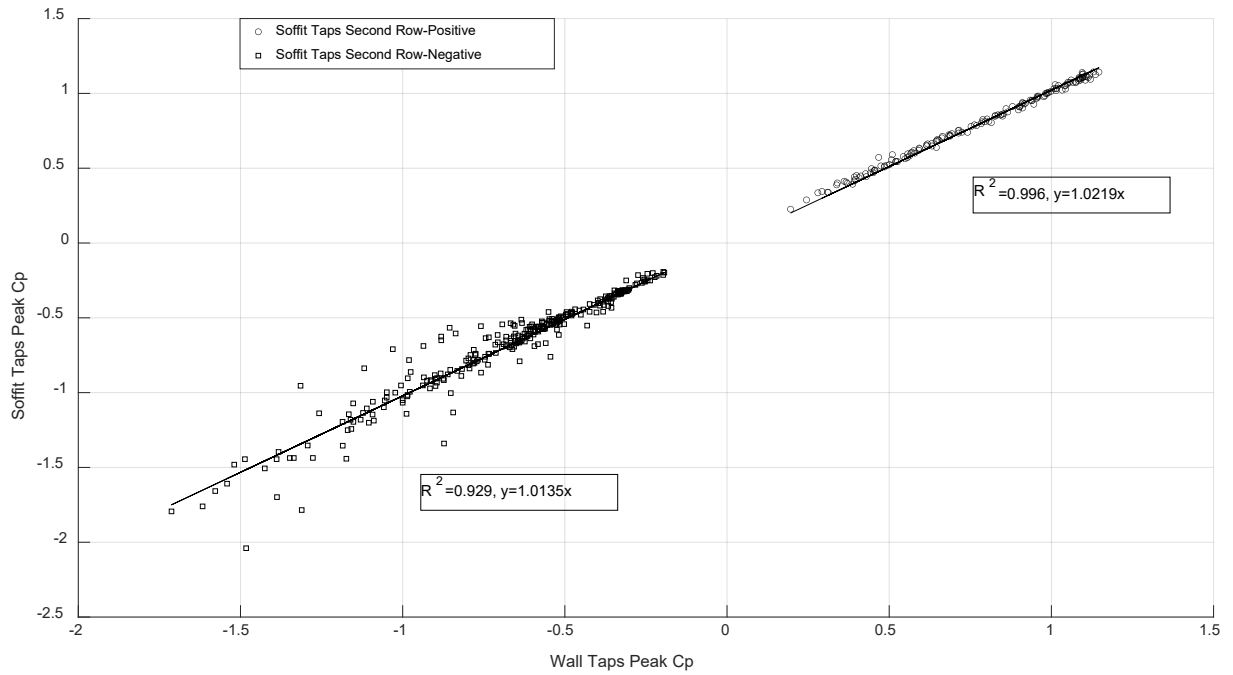
Figure 30 Linear Regression Relation between Upper Taps in South Wall and second row of taps in soffit for Model 'A'
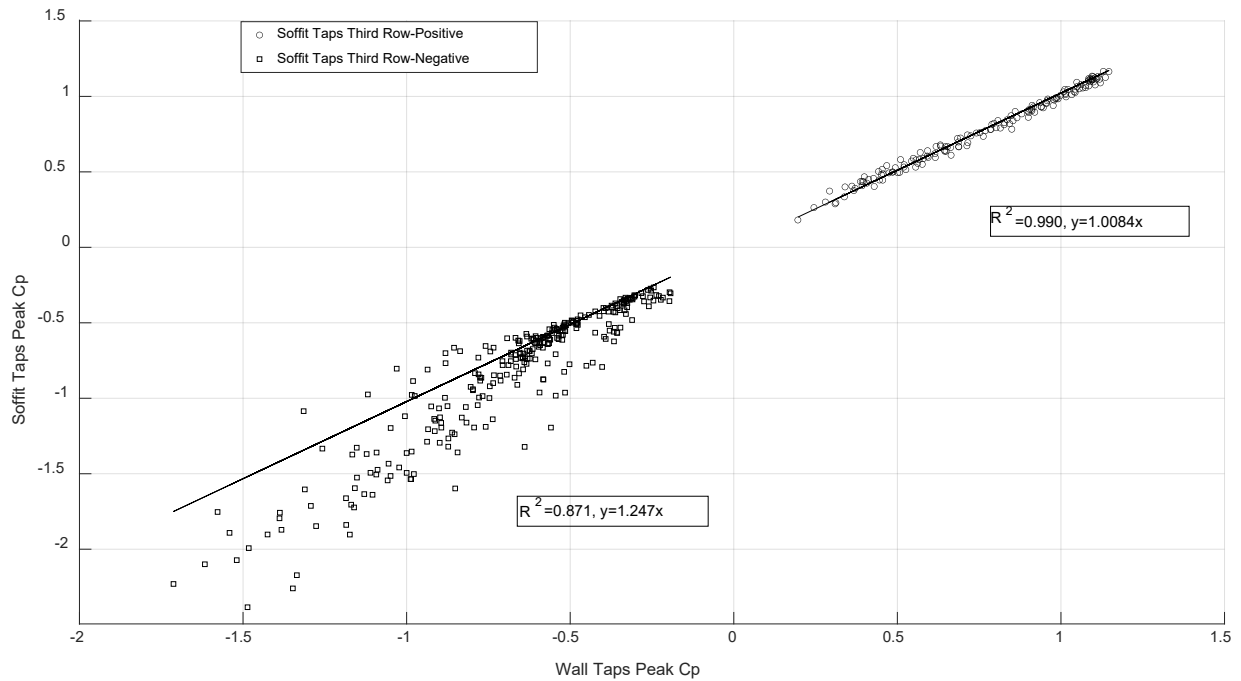
Figure 31 Linear Regression Relation between Upper Taps in South Wall and third row of taps in soffit for Model 'A'
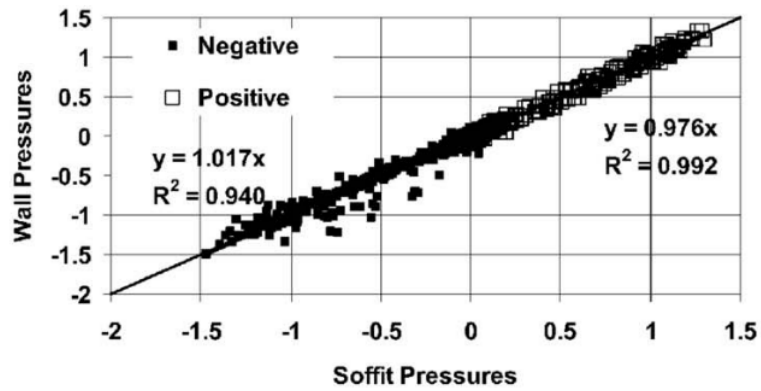
Figure 32 Soffit and wall pressure regression adapted from Vickery 2008.

Similarly, correlation coefficient and regression analysis were carried out for model B. The soffit taps were well correlated with the wall upper taps in wind directions that cause either predominant positive pressure on the taps (i.e., wind direction 135º to 225º) or predominant negative pressure (wake region at wind direction of 315º to 360º). For soffit taps located away from the wall, the correlation coefficient decreases. At wind direction of 100º and 110º, the soffit and wall taps were exposed to suction and the correlation coefficients of the edge taps decrease dramatically to a range of 0.1 to 0.2 as shown in Figure 33b. When the wall and the soffit are exposed to positive pressure, the soffit taps are well correlated with the wall taps, while exposing to suction, the soffit taps are not correlated with the walls. Therefore, this suggests that the pressure on the bottom covering of the roof overhang could be taken as the external pressure coefficient on the adjacent wall surface for positive Cp while for negative Cp, the relation should not be valid.

Figure 34 to Figure 38 show the regression analysis for south side between the upper wall taps and each row of the soffits taps. The regression slope for the five rows is slightly less than 1 which indicates that the pressure coefficient for the soffit taps were lower than that of the wall upper taps. This was counter to the regression line slope for model A, where the slopes were slightly greater than 1 and the Cp for soffit taps were slightly higher than that of the wall taps. As the taps located far from the wall, the correlation between the wall and taps significantly decrease and this is obvious in the regression analysis for the five rows of taps. The pressure coefficients are more divergent as the rows become far from the wall, and the R-squared values decrease significantly as well. This suggests that by increasing the overhang and the soffit length, the pressure coefficients at the soffit may decrease compared to the wall pressure coefficients.
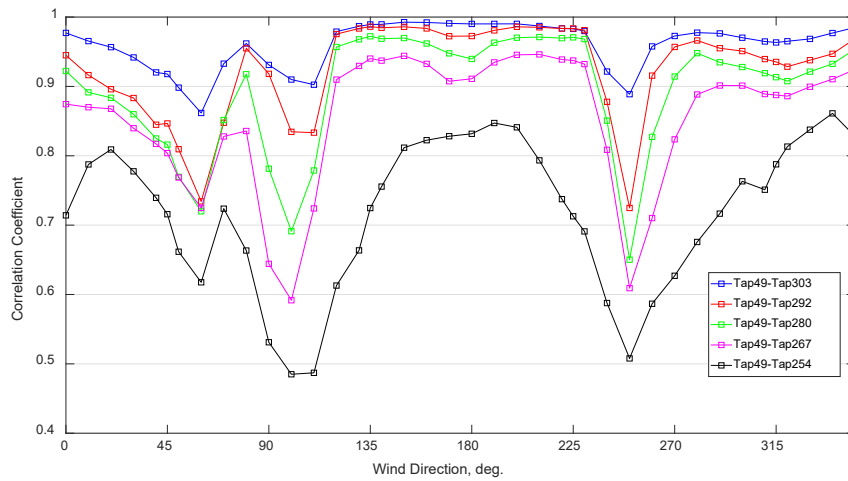
(a)
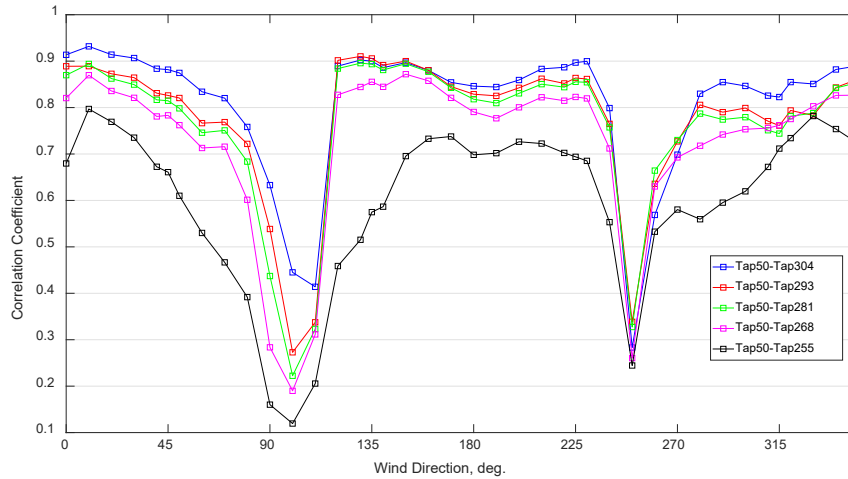
(b)
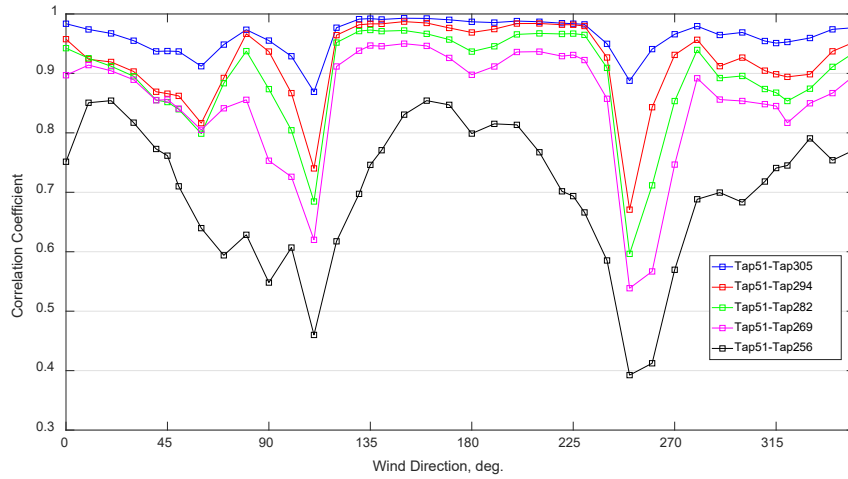
(c)

Figure 33 Correlation Coefficients between upper taps in wall (a) Tap 49 (b) Tap 50 (c) Tap 51 with adjacent taps in soffit.
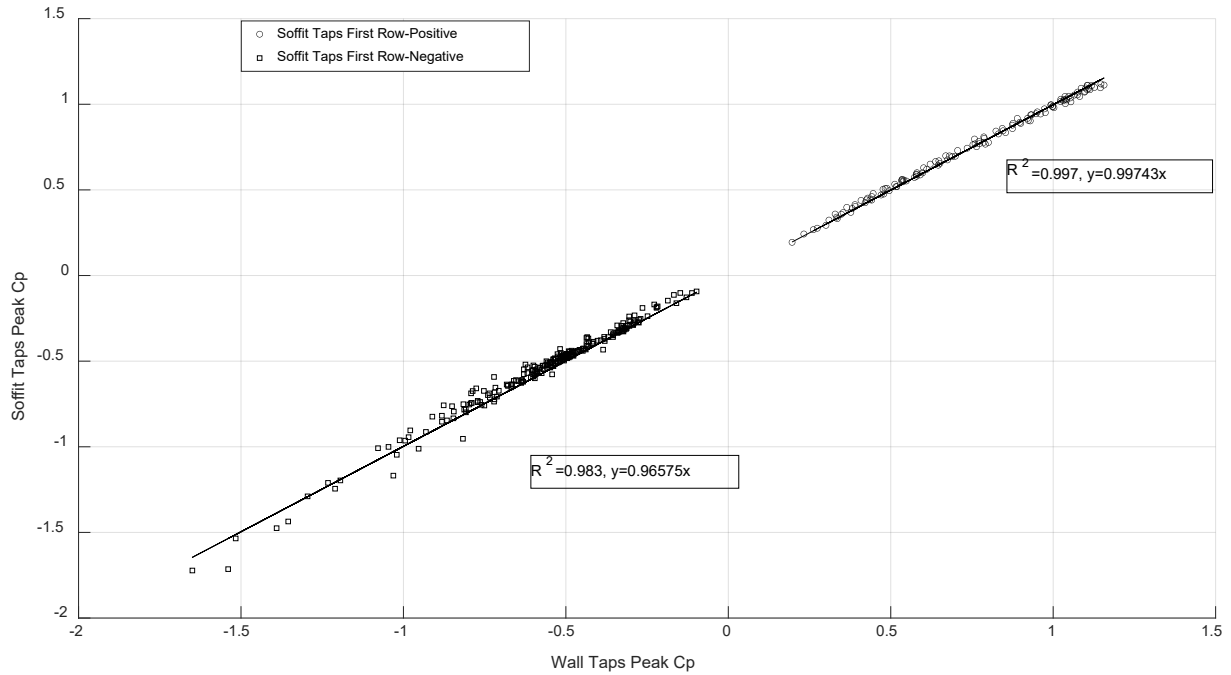
Figure 34 Linear Regression Relation between Upper Taps in South Wall and second row of taps in soffit for Model 'B'
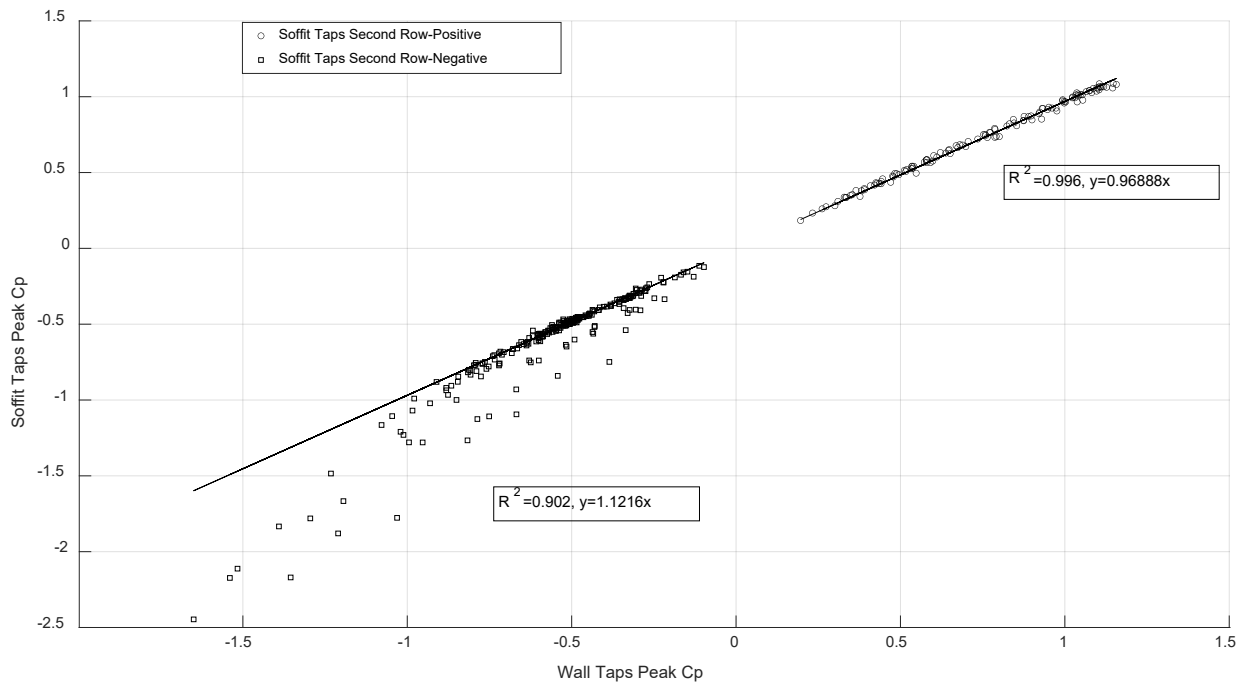
Figure 35 Linear Regression Relation between Upper Taps in South Wall and second row of taps in soffit for Model 'B'
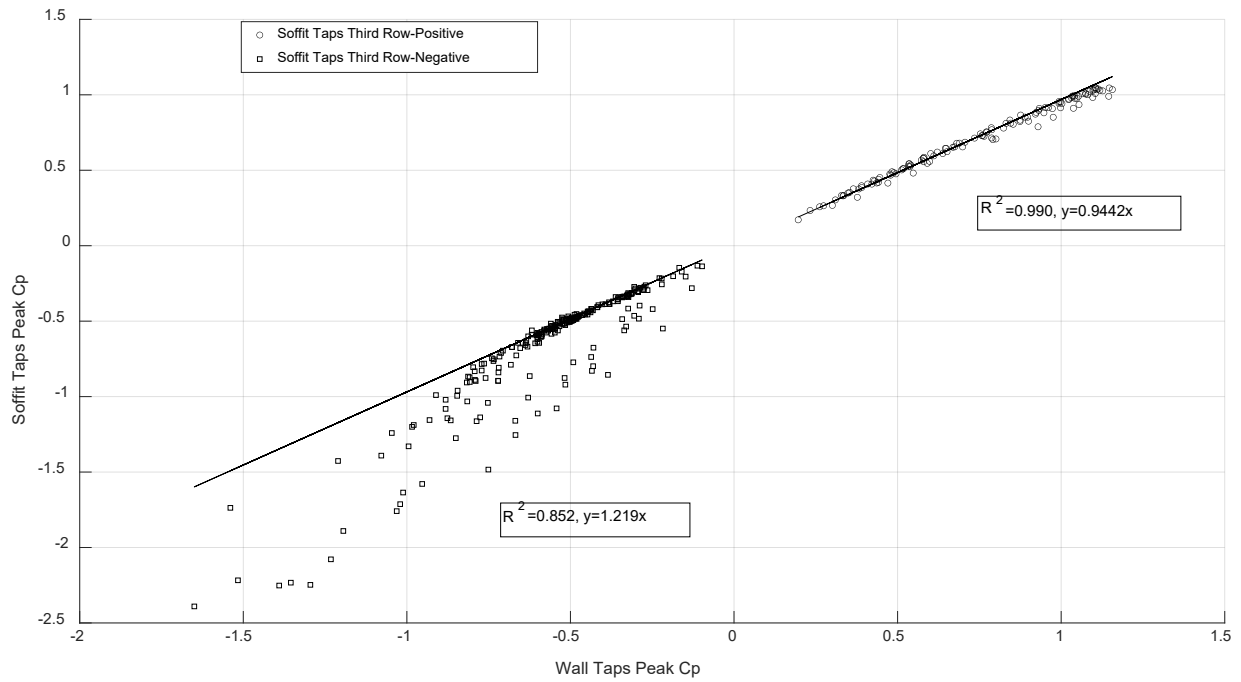
Figure 36 Linear Regression Relation between Upper Taps in South Wall and third row of taps in soffit for Model 'B'
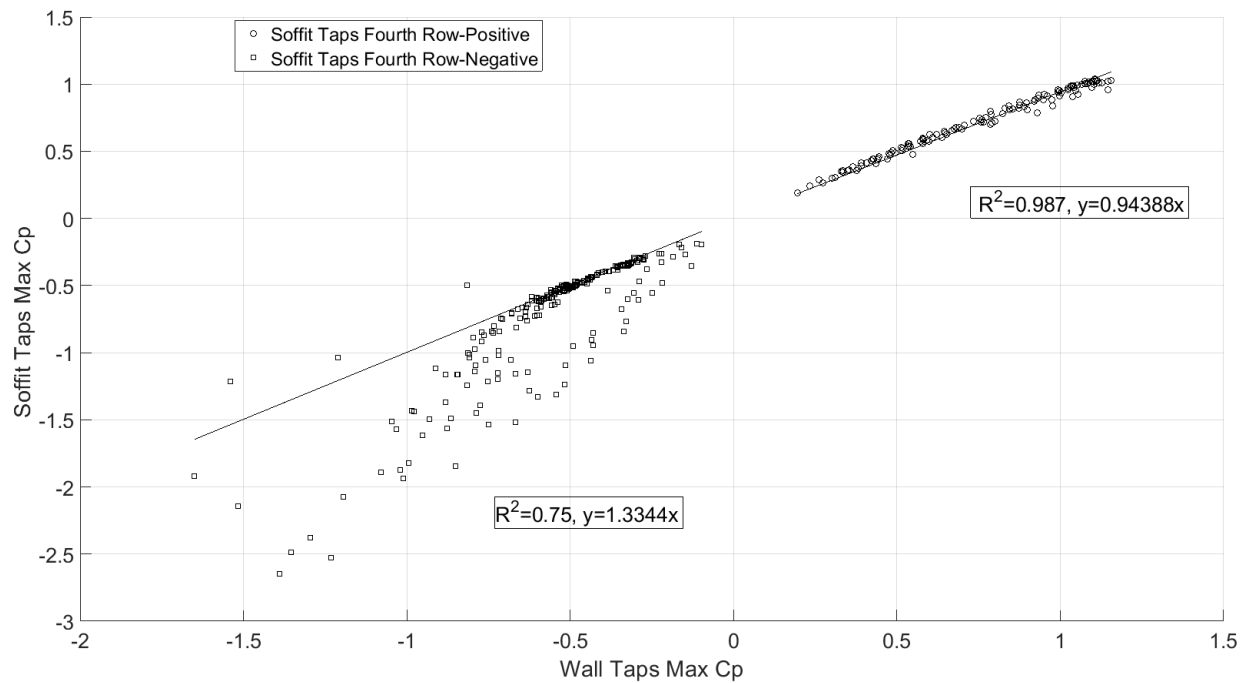
Figure 37 Linear Regression Relation between Upper Taps in South Wall and fourth row of taps in soffit for Model 'B'
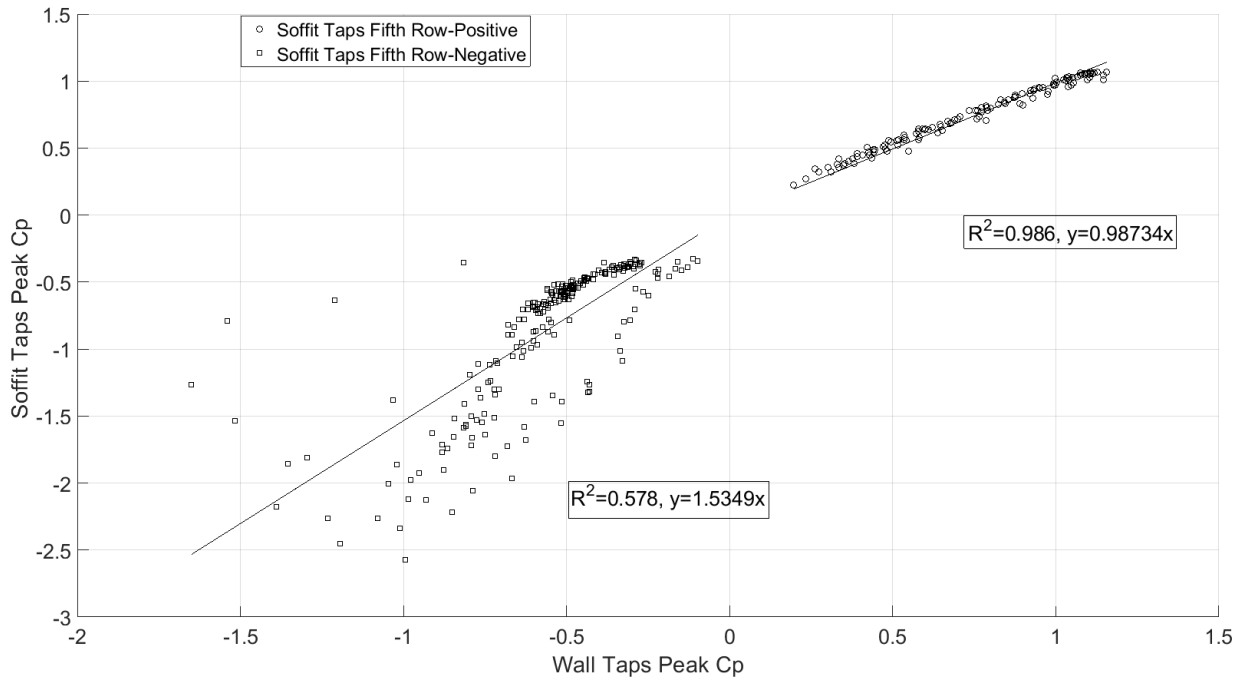
Figure 38 Linear Regression Relation between Upper Taps in South Wall and fifth row of taps in soffit for Model 'B'

Figure 39 and Figure 40 provide correlation coefficient contour plots for south soffit for both model A and model B, respectively, for five wind directions. As stated before, for all the soffit plots the wall side is the upper side of the plots, and the soffit edge is the lower side of the plots. Both cases show almost the same correlation coefficient when the models placed in the windward (180º degree). The correlation coefficients for case 1 are significantly higher at the outer edges compared to case 2, for all other shown directions. This indicates that the correlation coefficients for longer overhang significantly decrease compared to shorter overhangs, especially when the taps are exposed to suctions.
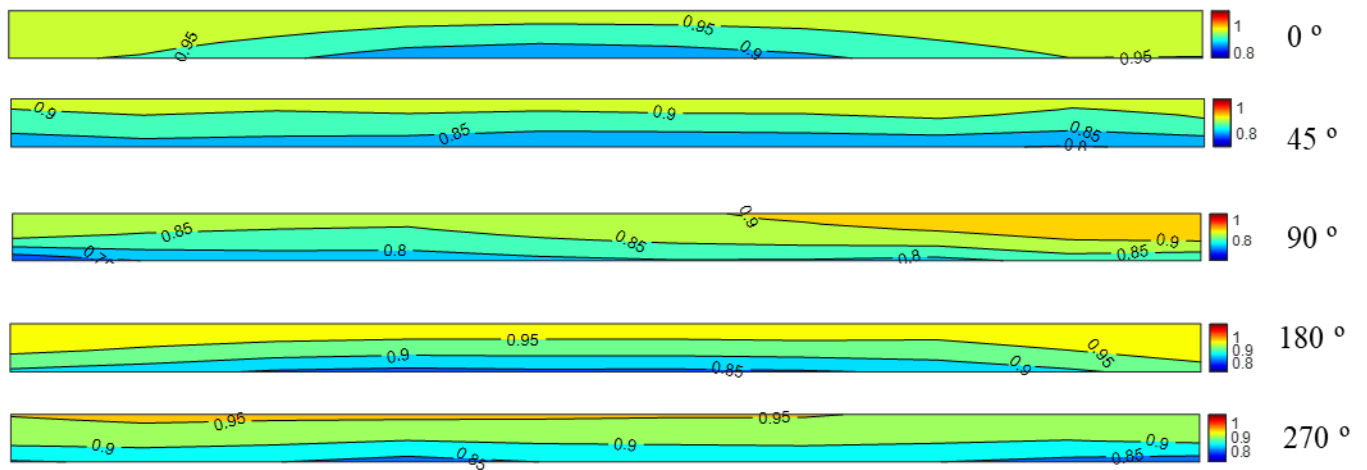
Figure 39 Correlation Coefficients contour plots for south soffit – Model A
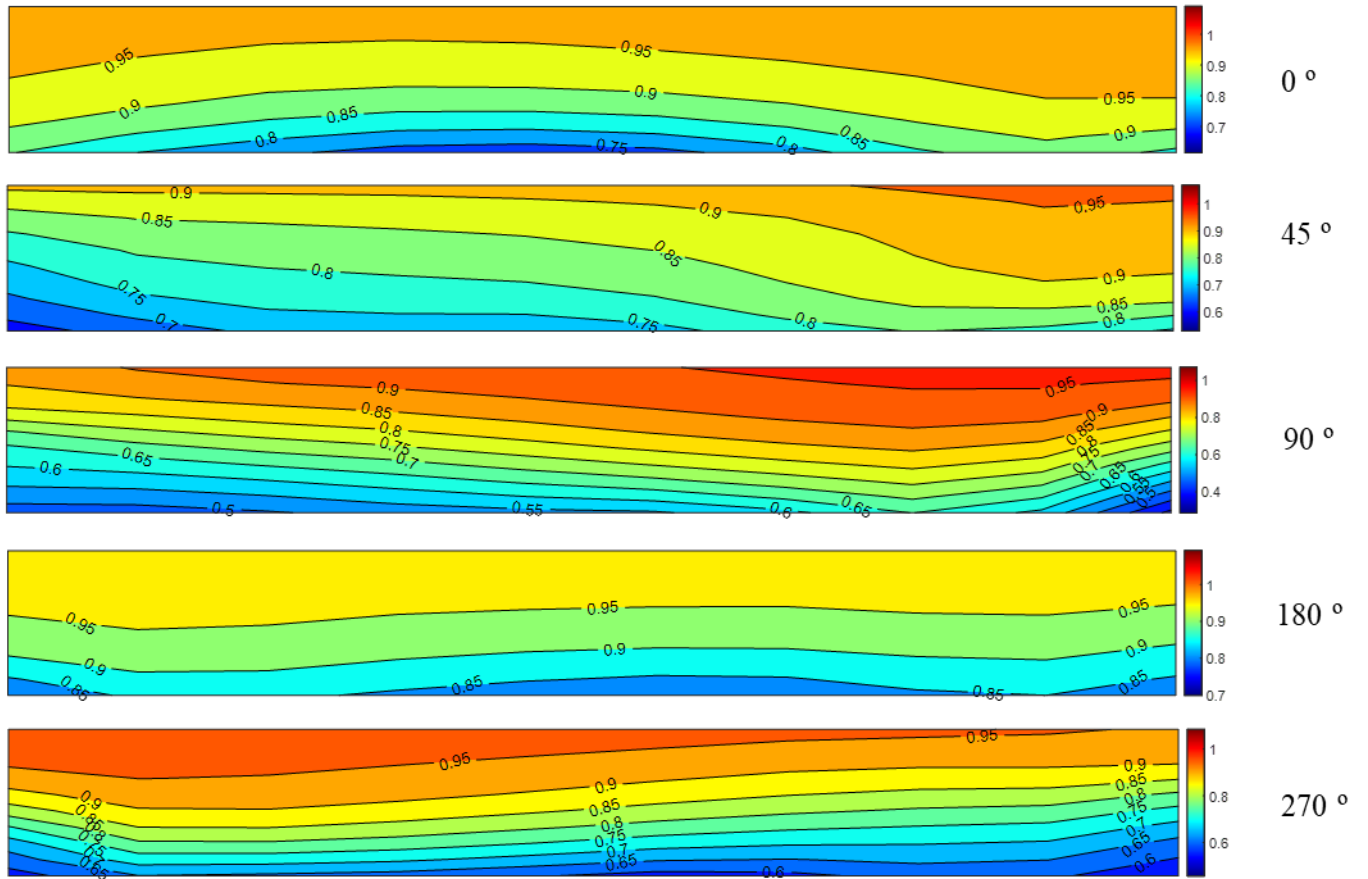
Figure 40 Correlation Coefficients contour plots for south soffit – Model B

5.4. Area Averaged pressure coefficients

In addition to the local pressure coefficient results that were discussed before, area-averaged values for combined pressure taps are necessary for codification purposes. The area averaged peak Cp were computed for each wind direction by considering single or multiple sets of pressure taps and assign them to their corresponding tributary area using equation 5. Area averaged pressure taps were considered according to the specified zones for hip roof of slope 7˚ to 20˚ in ASCE7-16 as shown in Figure 41.

$$Cp_{av} = \frac{\sum_i Cp_i \, A_i}{\sum_i A_i} \tag{5}$$
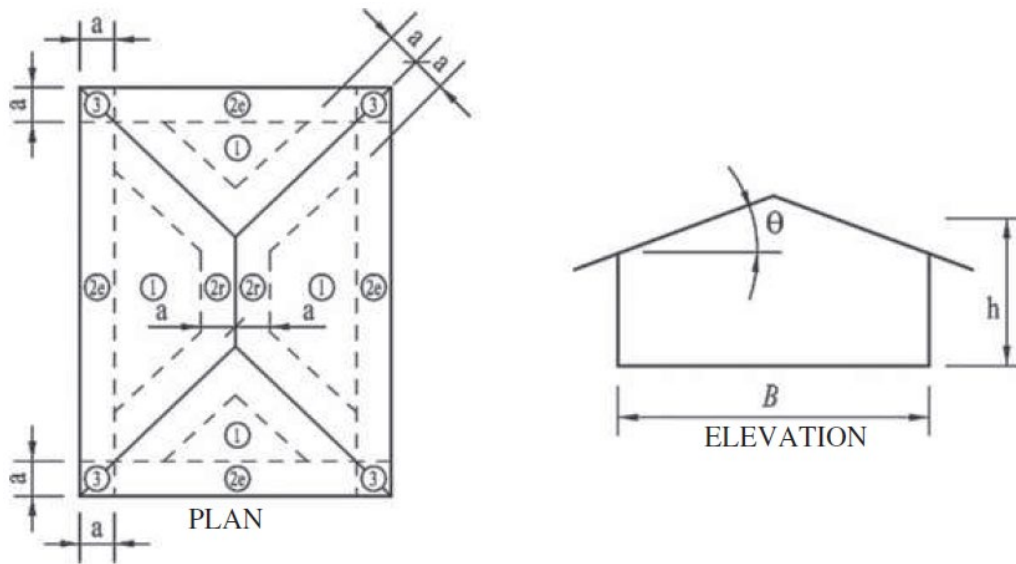
Figure 41 Zones specified for hip roof by ASCE7-16 (Adopted from FIGURE 30.3-2F in ASCE7-16)

Area averaged pressure analysis was done to investigate further the pressure scheme on portion or groups of taps on the overhangs when exposed to different wind directions. Pressure taps were placed in an orthogonal pattern, so according to (Simiu and Scanlan 1996) tributary area for orthogonal pressure taps are rectangular areas while for non-orthogonal patterns the tributary area could be calculated using Voronoi diagrams which could be derived from Delaunay triangulation. Figure 42 and Figure 43 show the different area averaged combination for pressure taps on south and east roof, respectively for model A.
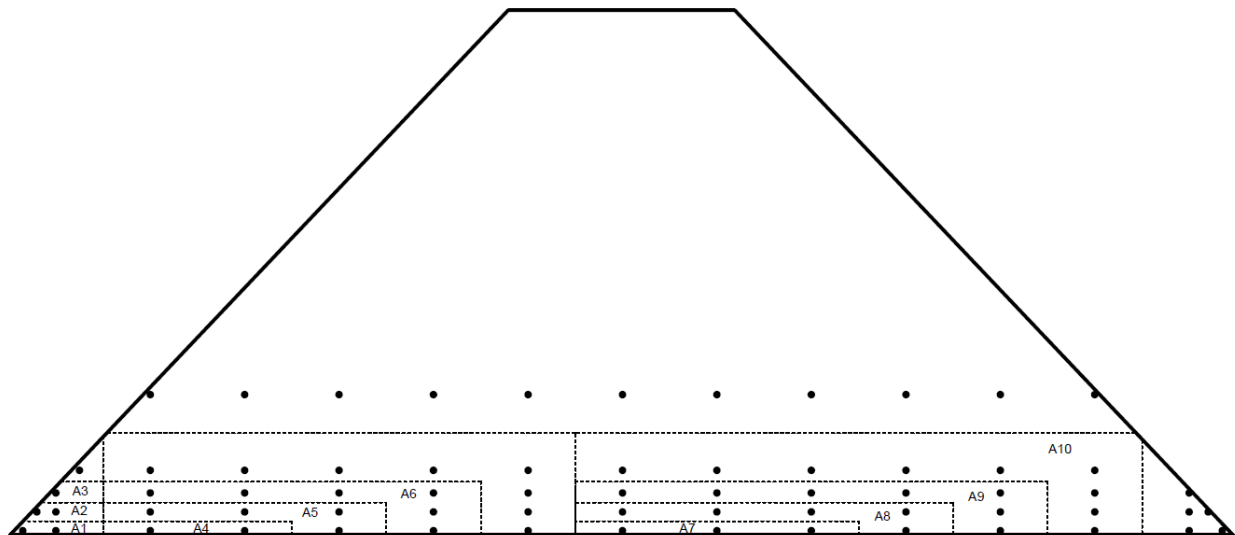
Figure 42 Different Areas used for area averaged loads for south roof for Model A
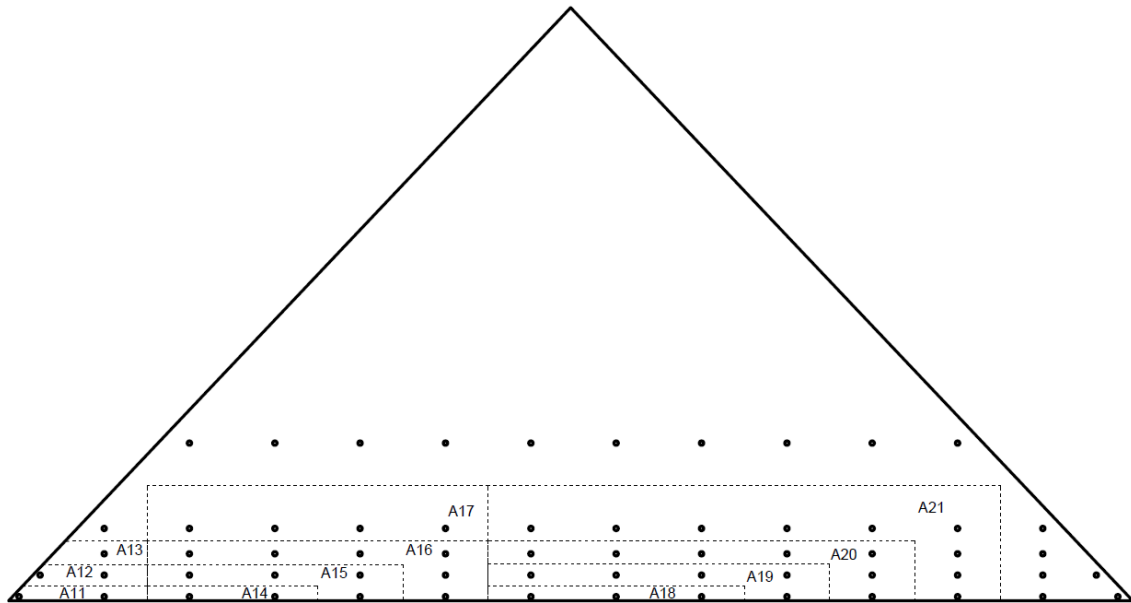
Figure 43 Different Areas used for area averaged loads for south roof for Model B.

Figure 44 and Figure 45 comprise of the experimental results of overhang's peak external pressure coefficient in terms of effective area and without considering any reduction factor. One plot corresponds to the south side and the other to the east side of the models. In ASCE7-16, there are two GCp plots for gable roof of slope 7° to 20° with overhangs, one for h/B ≥ 0.8 and the other for h/B ≤ 0.5. According to the dimension of both models (40 ft x 50 ft x 28.75 ft), h/B for south side is 0.57 and for east side is 0.72. Consequently, interpolation plots were made to account for both h/B.

Both plots show the expected monotonically decreasing relationship between the effective area and the magnitude of the external pressure coefficients. For the east side in both models, almost all magnitudes of peak external GCp were below the limitations of zone 3 and 2e. In contrast, for south side, magnitudes of most of the sets in zone 2e were above the limits and magnitudes of zone 3 were below the limits for case 1. While, for case 2 south side, magnitudes for most of the sets were below the limits for zone 2e and 3, this is summarized in Table 6. This may suggest that ASCE7-16 is less conservative regarding zone 2e. The GCp plots in ASCE7-16 were formed based on small scale wind tunnel testing, where Reynold's number is usually being violated and smaller number of pressure taps is used. Nonetheless, more testing configurations are needed to confirm that finding.

Table 6 summary for peak Cp compared to GCp limits in ASCE7-16 for different zones.

Case	Side	Zone 3	Zone 2e
1 (Model A)	East	Within ASCE7-16 limits	Within ASCE7-16 limits
	South	Within ASCE7-16 limits	*Above ASCE7-16 limits*
2 (Model B)	East	Within ASCE7-16 limits	Within ASCE7-16 limits
	South	Within ASCE7-16 limits	Within ASCE7-16 limits
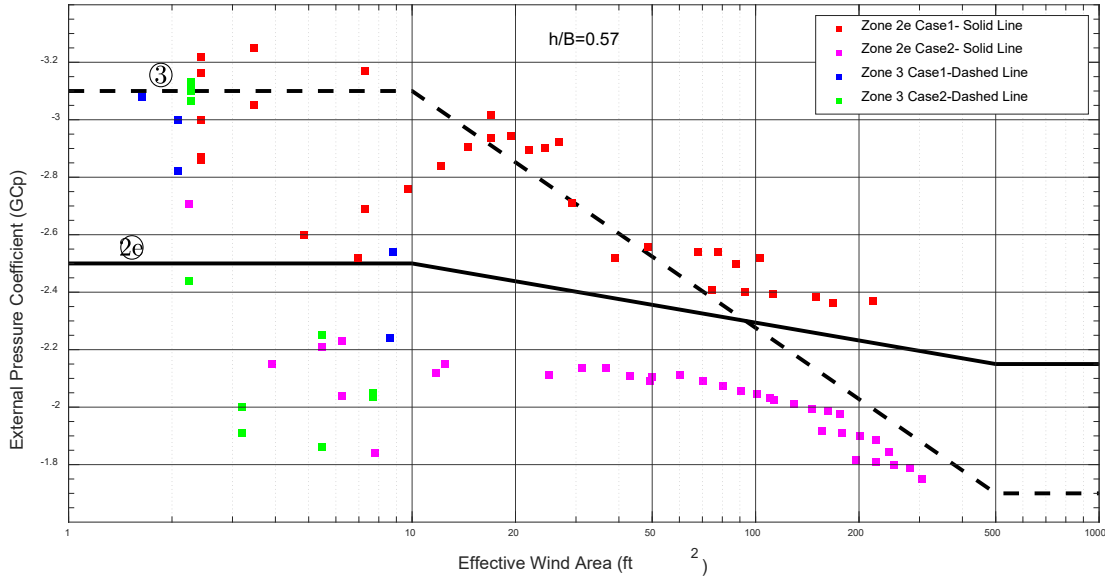
Figure 44 Critical area-averaged external pressure coefficient for south side compared to GCp plot in ASCE7-16.
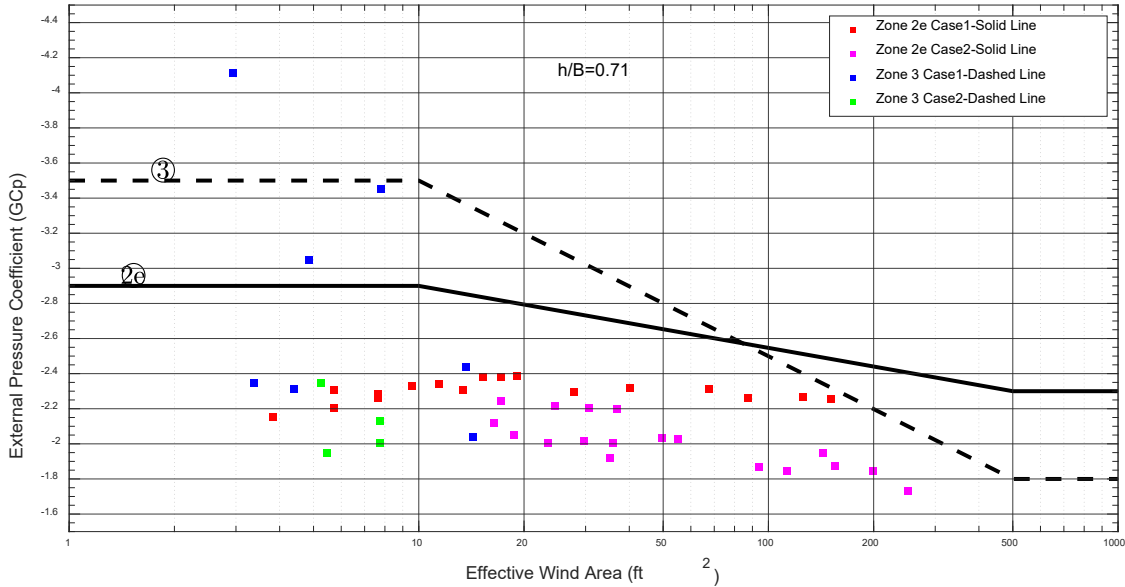
Figure 45 Critical area-averaged external pressure coefficient for east side compared to GCp plot in ASCE7-16.

6. Overall summary, conclusion and future works

6.1. Summary

Large scale wind tunnel experiments were conducted at the Wall of Wind at Florida International University for two configurations of a residential building of hip roof with different overhang length. Peak local surface wind coefficients were measured for walls, soffits, and roofs with overhangs for both configuration cases. Moreover, area averaged pressure coefficients were measured for different combinations of taps and were compared to the GCp plots in ASCE7-16. In addition to local and area averaged pressure coefficients, correlation coefficients and regression analysis was considered to assess the correlation of soffit pressure coefficients to pressure coefficients of wall upper taps. The findings show that the 2 ft overhang experienced higher suction coefficients at the edges compared to the 6 ft overhang. In addition, the results confirmed that, for both configurations, soffit pressure coefficients may be taken as the adjacent wall external pressure, as stated by ASCE7-16. The length of the overhang did not seem to have a considerable effect on the positive pressure coefficient on walls and soffit. However, by carrying out correlation analysis and regression analysis between soffit pressure taps and upper wall taps, the 6 ft soffit seemed to be less correlated with the wall upper taps, than the 2 ft soffit. Area averaging and pressure coefficients for overhangs, and adjacent roof areas were compared to the GCp plots in ASCE 7-16 for each specified zone. Results were within the limits of the provisions for zone 3, while it is apparent that the Standard is less conservative regarding zone 2e.

6.2. Conclusions

Based on experimental testing results and discussion, the following concluding remarks can be drawn:

- The 2 ft inclined overhangs were found to have higher pressure coefficient at the edges compared to the 6 ft overhangs.
- The effect of roughness did not seem to have a considerable effect on pressure coefficients on roof and overhangs, while for walls the effect of roughness seemed to be more considerable.
- Pressure taps at the soffit edge exposed to higher peak min Cp compared to the middle and inner taps.
- The pressure coefficients at the soffit were slightly higher than the wall pressure coefficients in 2 ft overhangs and slightly lower in case of 6 ft overhangs.
- The length of the overhang did not seem to have a considerable effect on the absolute positive pressure correlation between walls and soffits.
- The length of the overhang has a recognized effect on the negative pressure correlation between walls and soffits.
- The 6 ft soffit seemed to be less correlated at the edge with the wall upper taps compared to the 2 ft soffit.
- The correlation coefficients for longer soffits with the wall significantly decrease compared to shorter soffits when the walls and soffits are exposed to suctions.

- The soffit pressure coefficients should be taken as the adjacent wall external pressure, as stated by ASCE7-16 for positive pressure only, while this shall not be applicable for suction pressure.
- GCp plots in ASCE7-16 for hip roof of slope 7º to 20º maybe less conservative regarding zone 2e.

6.3. Future work

More configurations need to be tested as a large-scale testing that include different construction methods and geometries used in low-rise building stock for verifying GCp plots in ASCE7-16. Only limited amount of testing cases was conducted in this phase which did not allow to proceed with a detailed codification process, that can lead to potentially valuable design recommendation for enhancement of future wind standards and building codes of practice. The different construction methods may include overhangs without soffit to assess the performance of overhangs under net Cp as shown in Figure 46. In addition, buildings with gable roof and hip roof of different slopes would be included in next phase of testing. If it applicable the existing and new configurations could be tested under different types of wind events (i.e., synoptic and non-synoptic) to assess the performance of overhangs.
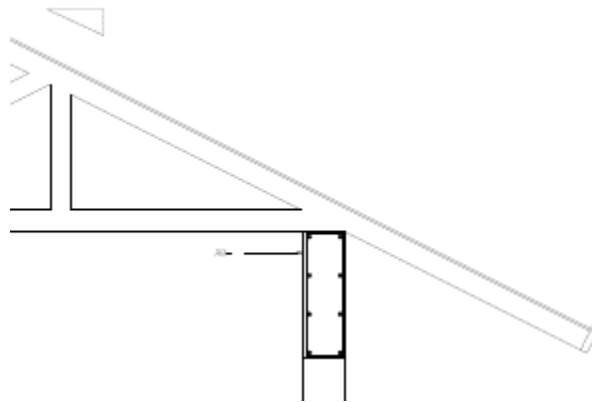
Figure 46 Structural detail of overhang without soffit.

References

Ahmad, S., and Kumar, K. (2002). "Effect of geometry on wind pressures on low-rise hip roof buildings." *Journal of Wind Engineering and Industrial Aerodynamics*. Vol. 90 (7), 755-779.

ASCE. (2010). "Minimum design loads for building and other structures." American Society of Civil Engineers, ASCE/SEI 7-10, Reston, VA.

ASCE. (2017). "Minimum Design Loads and Associated Criteria for Buildings and Other Structures." American Society of Civil Engineers, ASCE/SEI 7-16, Reston, VA.

Candelario, J. D., Stathopoulos, T., and Zisis, I. (2014). "Wind Loading on Attached Canopies: Codification Study." *Journal of Structural Engineering*, 140(5), 04014007.

Gan Chowdhury, A., Zisis, I., Irwin, P., Bitsuamlak, G., Pinelli, J.-P, Hajra, B., and Moravej, M. (2017). "Large-Scale Experimentation Using the 12-Fan Wall of Wind to Assess and Mitigate Hurricane Wind and Rain Impacts on Buildings and Infrastructure Systems." *Journal of Structural Engineering*, Vol. 143, Issue 7.

Ho, T. C. E., Surry, D., Morrish, D., and Kopp, G. A. (2005). "The UWO contribution to the NIST aerodynamic database for wind loads on low buildings: Part 1. Archiving format and basic aerodynamic data." *Journal of Wind Engineering and Industrial Aerodynamics*, 93(1), 1–30.

Huang, P., Tao, L., Gu, M., and Quan, Y. (2018). "Experimental study of wind loads on gable roofs of low-rise buildings with overhangs." *Frontiers of Structural and Civil Engineering*, 12(3), 300–317.

Irwin, H., Cooper, K. R., and Girard, R. (1979). "Correction of distortion effects caused by tubing systems in measurements of fluctuating pressures." *Journal of Wind Engineering and Industrial Aerodynamics,* Elsevier, 5(1–2), 93–107.

John, A. D., Gairola, A., and Krishna, P. (2008). "Wind Loads on Overhangs in a Low Gable Building in Presence of Free Standing Wall." *Journal of Wind and Engineering*, 5(1), 39–46.

John, A. D., Singla, G., Shukla, S., and Dua, R. (2011). "Interference effect on wind loads on gable roof building." *Procedia Engineering*, Elsevier B.V., 14, 1776–1783.

Kozmar, H. (2021). "Flow, turbulence and surface pressure on a wall-mounted cube in turbulent boundary layers." *Journal of Wind Engineering and Industrial Aerodynamics*, Elsevier Ltd, 210(February), 104503.

Milne, I. A., Sharma, R. N., Flay, R. G. J., and Bickerton, S. (2013). "Characteristics of the turbulence in the flow at a tidal stream power site." *Philosophical Transactions of the Royal Society A: Mathematical, Physical and Engineering Sciences*, 371(1985).

Mooneghi, M. A., Irwin, P., and Chowdhury, A. G. (2016). "Partial turbulence simulation method for predicting peak wind loads on small structures and building appurtenances." *Journal of Wind Engineering and Industrial Aerodynamics*, Elsevier, 157, 47–62.

Moravej, M. (2018). "Investigating scale effects on analytical methods of predicting peak wind loads on buildings." Florida International University.

Saathoff, P. J., and Melbourne, W. H. (1997). "Effects of free-stream turbulence on surface pressure fluctuations in a separation bubble*." Journal of Fluid Mechanics*, Florida International Uni, 337, 1–24.

Stathopoulos, T. (1981). "Wind Loads on Eaves of Low Buildings." *ASCE J Struct Div.*

Stathopoulos, T., and Luchian, H. (1994). "Wind-induced forces on eaves of low buildings." *Journal of Wind Engineering and Industrial Aerodynamics*, 52(C), 249–261.

St. Pierre, L. M., Kopp, G. A., Surry, D., and Ho, T. C. E. (2005). "The UWO contribution to the NIST aerodynamic database for wind loads on low buildings: Part 2. Comparison of data with wind load provisions." *Journal of Wind Engineering and Industrial Aerodynamics*, 93(1), 31–59.

Taher, R. (2007). "Design of Low-Rise Buildings for Extreme Wind Events." *Journal of Architectural Engineering*, 13(1), 54–62.

Vickery, P. J. (2008). "Component and Cladding Wind Loads for Soffits." *Journal of Structural Engineering*, 134(5), 846–853.

Wiik, T., and Hansen, E. W. M. (1997). "The assessment of wind loads on roof overhang of low-rise buildings." *Journal of Wind Engineering and Industrial Aerodynamics*, 67–68, 687–696.

Wang, X., Li, Q., and Li, J. (2020). "Field monitoring and wind tunnel study of wind effects on roof overhang of a low-rise building." *Structural Control and Health Monitoring*, 27(3), 1–25.

Zisis, I., and Stathopoulos, T. (2010). "Wind-Induced Pressures on Patio Covers." *Journal of Structural Engineering*, 136(9), 1172–1181.

Zisis, I., Raji, F. and Candelario, J. D. (2017). "Large scale wind tunnel tests of canopies attached to low-rise buildings." *ASCE Journal of Architectural Engineering*, Vol. 23 (1).

Appendix A- Peak Max/Min Cp

Case 1- East Side at WD of 180 Degree-Open terrain
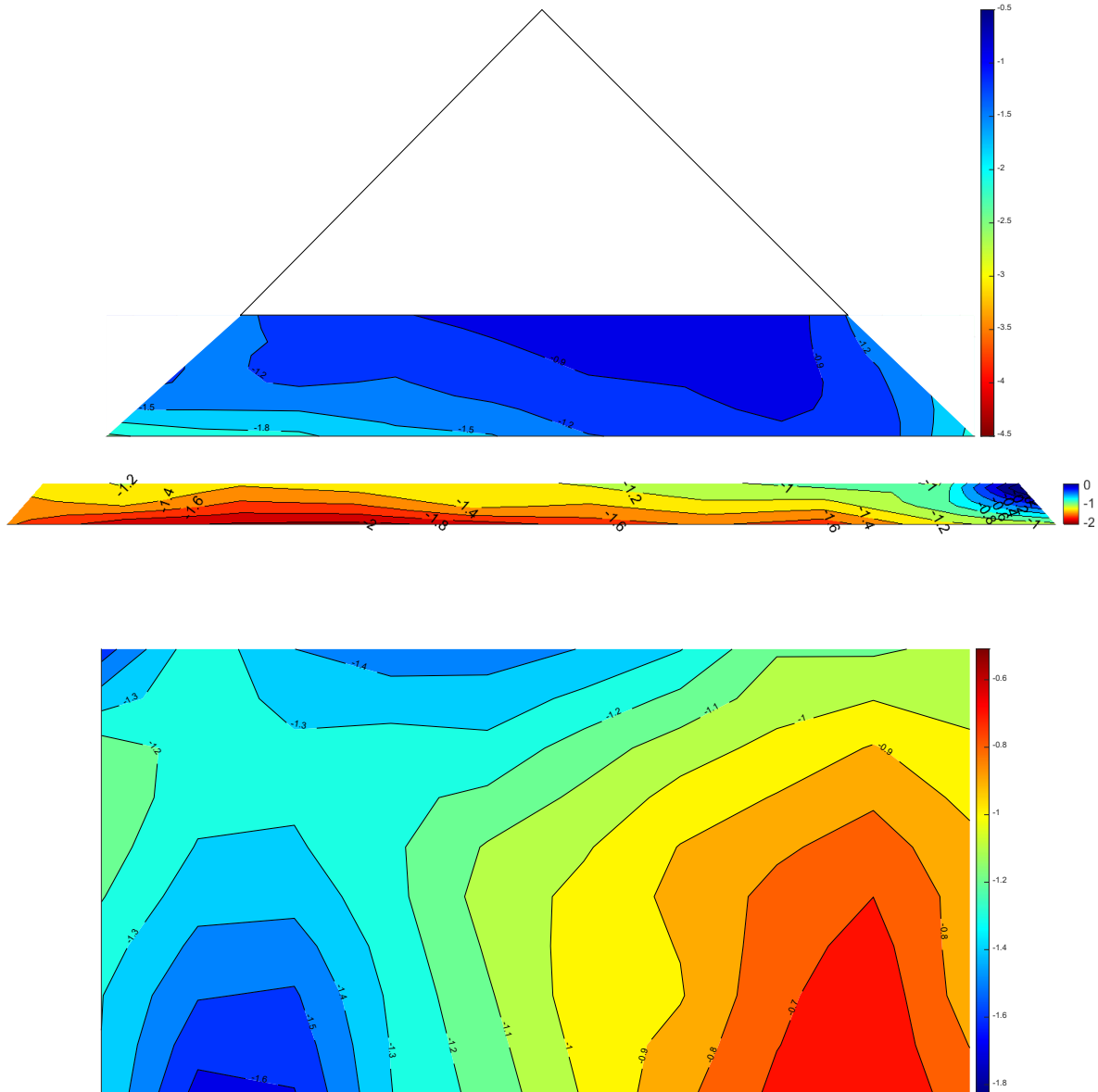
Figure 47 Peak Min Cp for roof and Peak Max Cp for wall and soffit for East Side of Model A at wind direction of 180° Open Terrain

Case 1- South Side at WD of 90 Degree
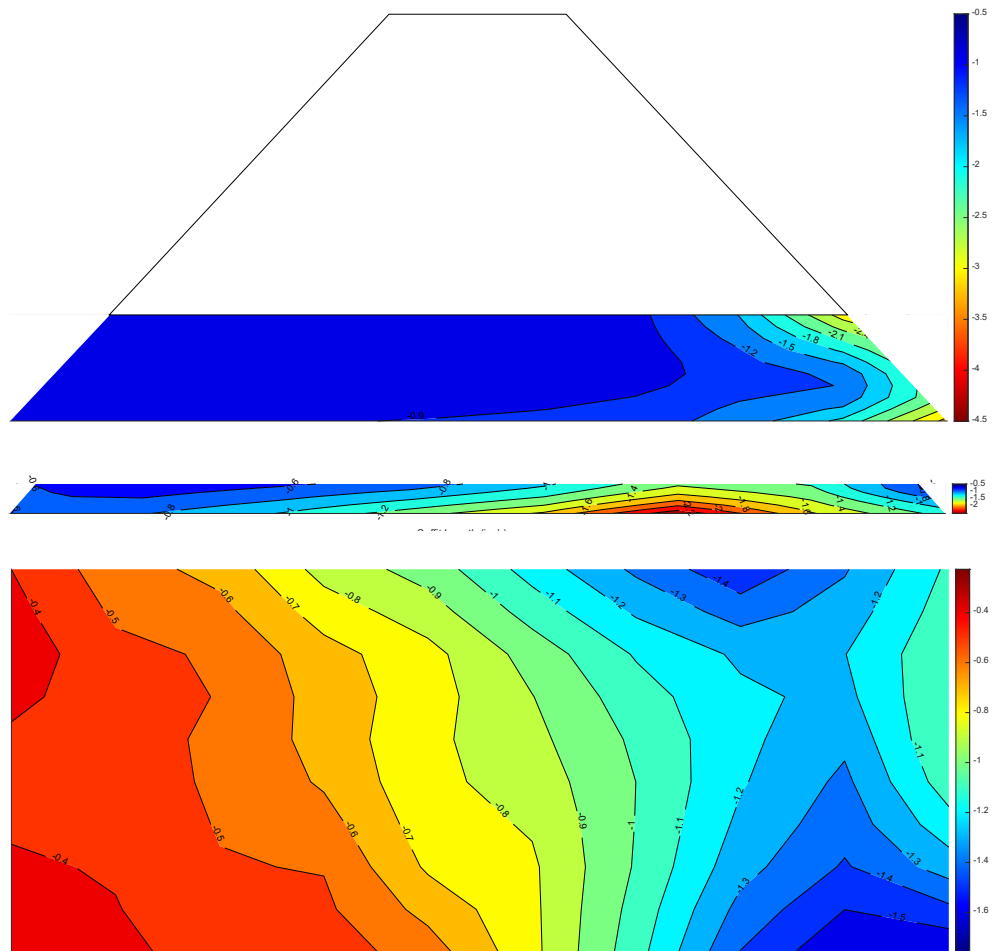
Figure 48 Peak Min Cp for roof and Peak Max Cp for wall and soffit for South Side of Model A
at wind direction of 90˚ Open Terrain

Case 1- East Side at WD of 90 Degree
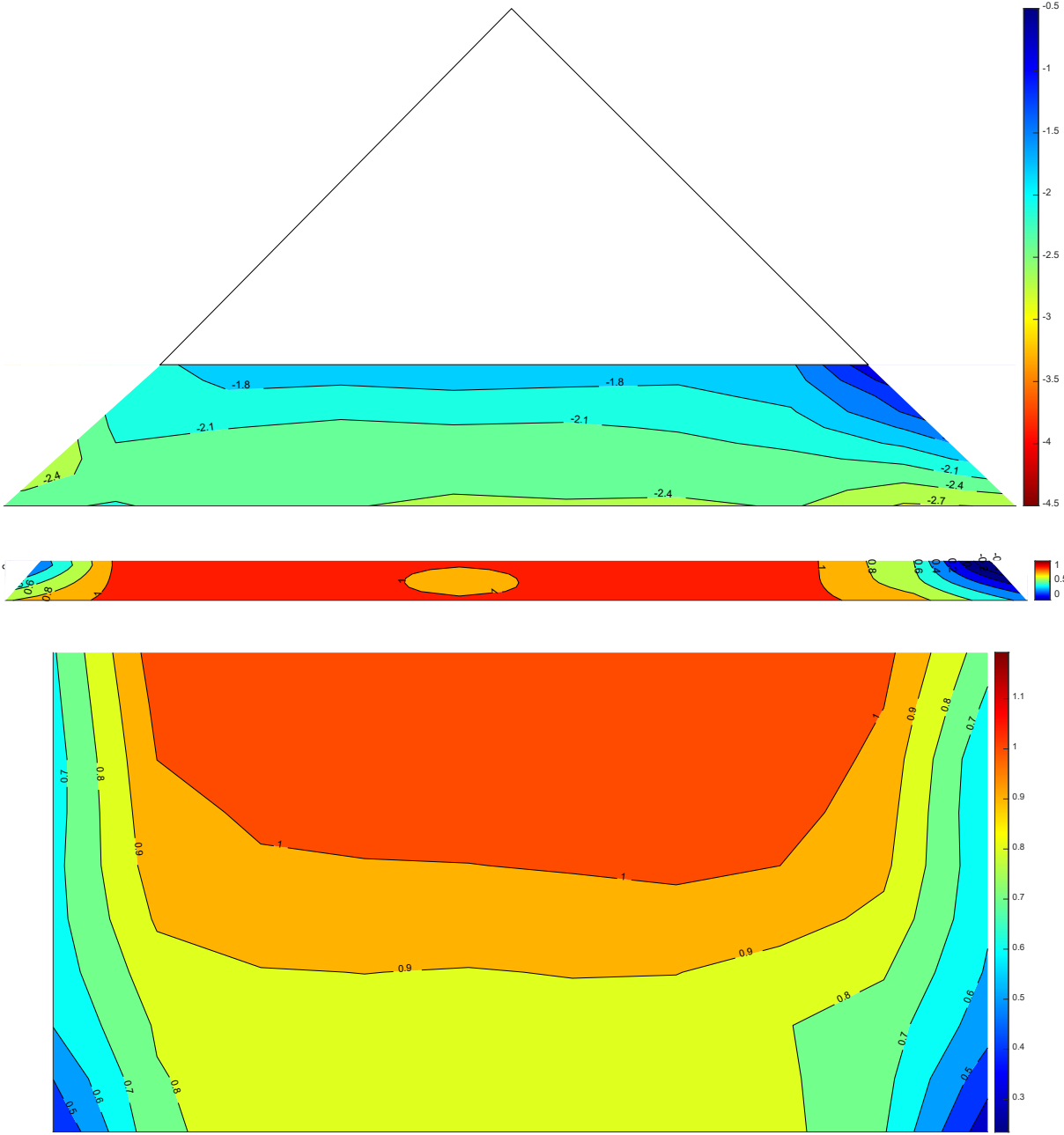
Figure 49 Peak Min Cp for roof and Peak Max Cp for wall and soffit for East Side of Model A at wind direction of 90° Open Terrain

Case 1- South Side at WD of 135 Degree
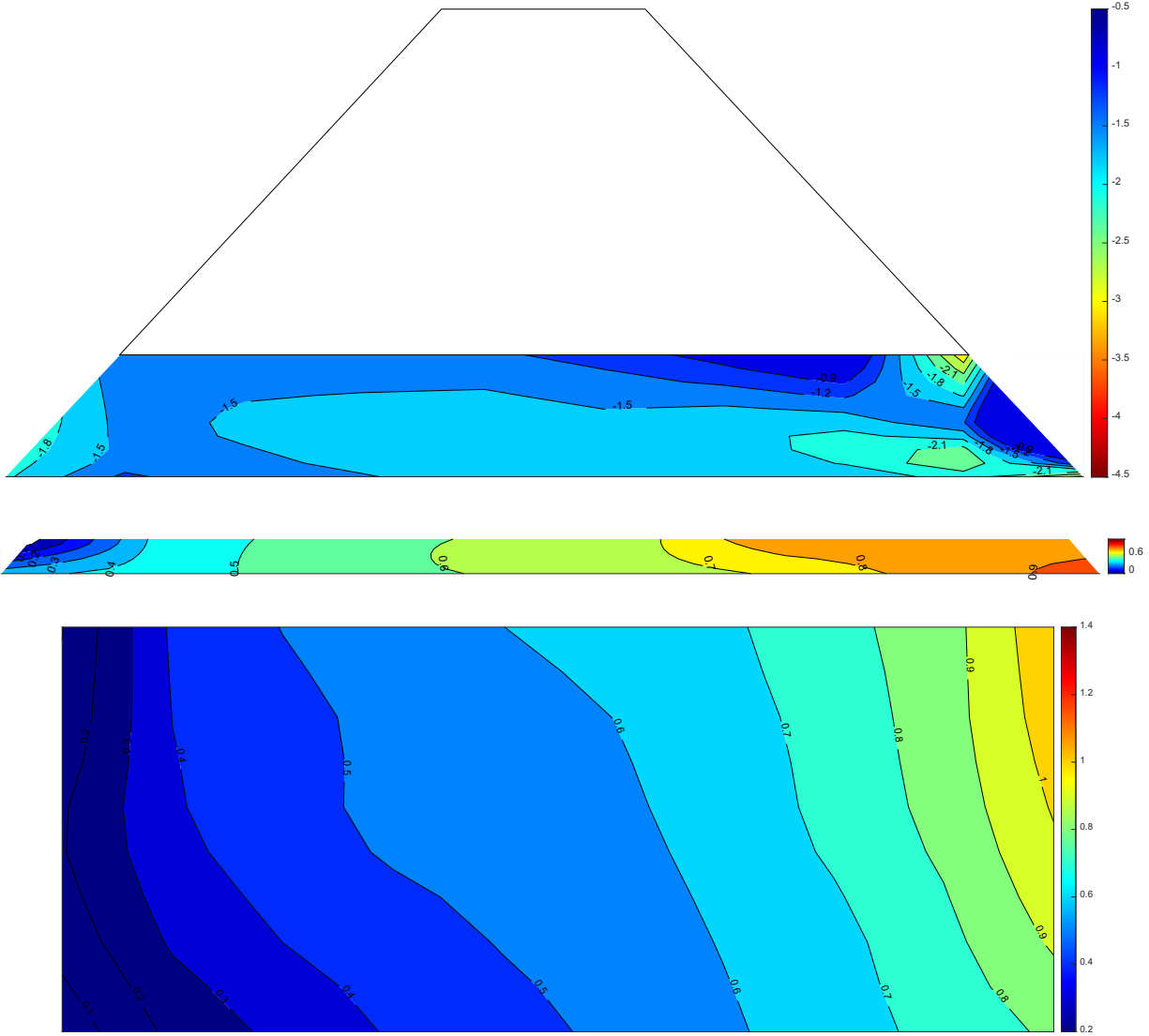
Figure 50 Peak Min Cp for roof and Peak Max Cp for wall and soffit for South Side of Model A at wind direction of 135˚ Open Terrain

Case 1- East Side at WD of 135 Degree
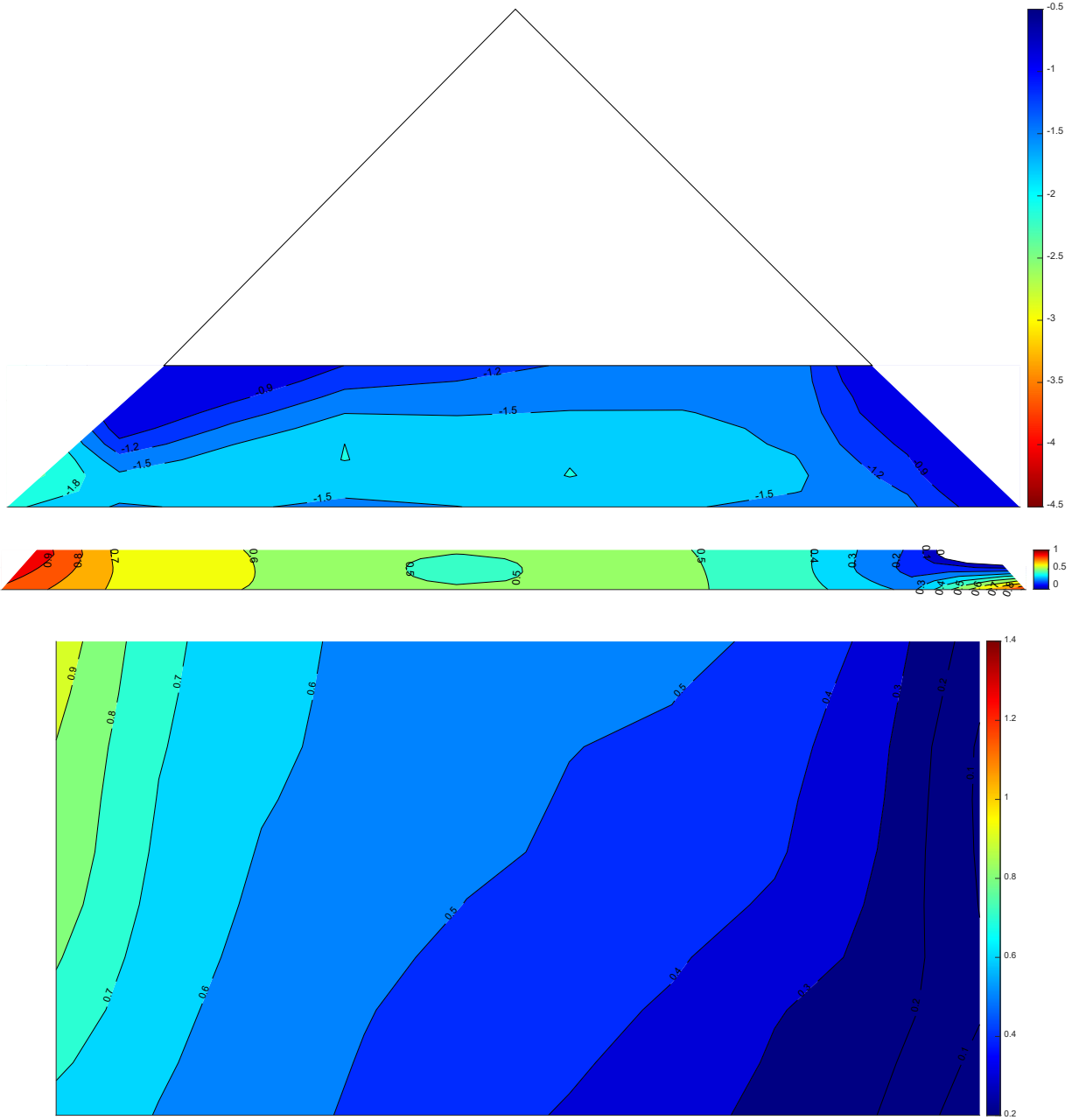
Figure 51 Peak Min Cp for roof and Peak Max Cp for wall and soffit for East Side of Model A at wind direction of 135˚ Open Terrain

Case 2- East Side at WD of 180 Degree
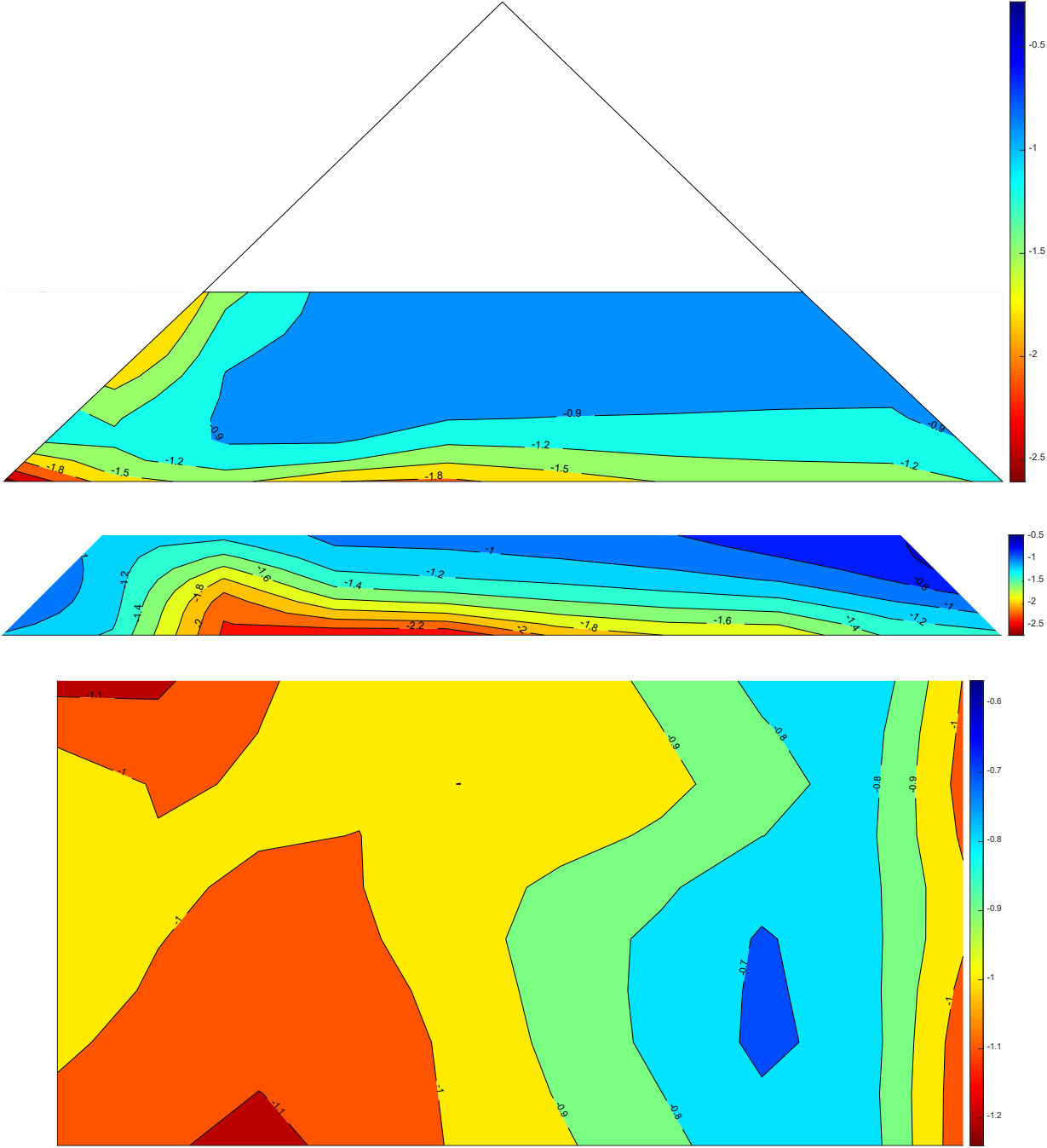
Figure 52 Peak Min Cp for roof and Peak Max Cp for wall and soffit for East Side of Model B at wind direction of 180° Open Terrain

Case 2- South Side at WD of 90 Degree
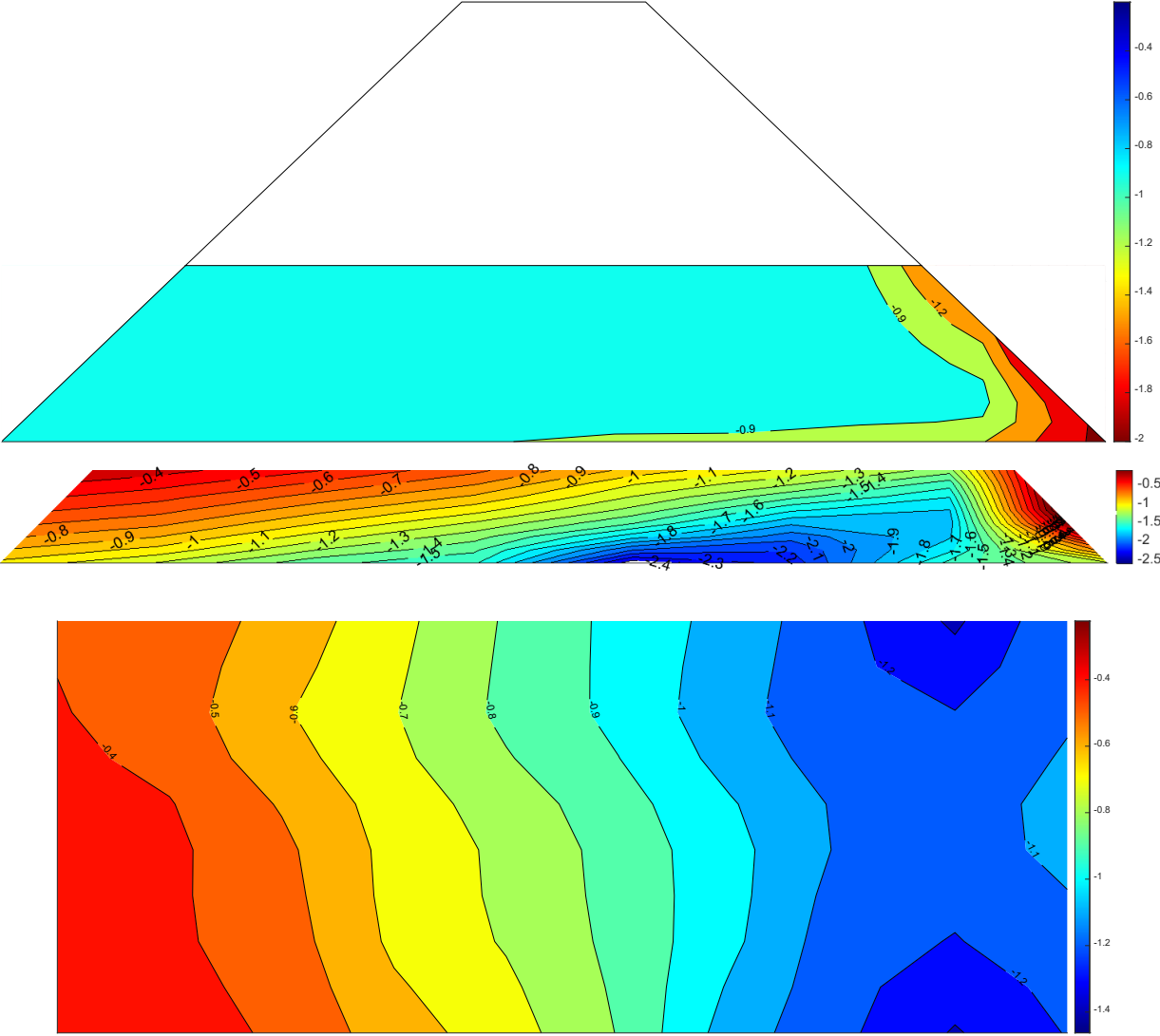
Figure 53 Peak Min Cp for roof and Peak Max Cp for wall and soffit for South Side of Model B
at wind direction of 90˚ Open Terrain

Case 2- East Side at WD of 90 Degree
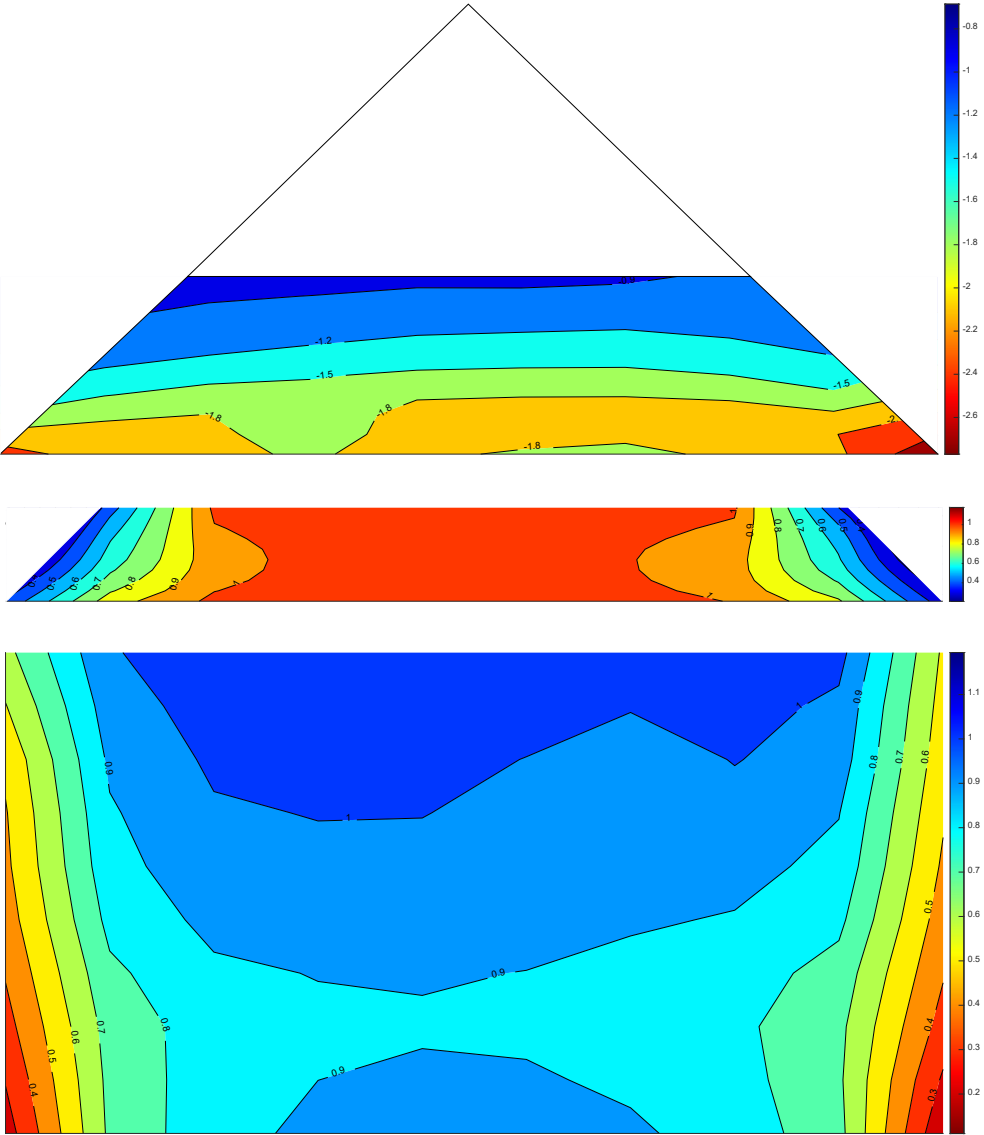
Figure 54 Peak Min Cp for roof and Peak Max Cp for wall and soffit for East Side of Model B at wind direction of 90° Open Terrain

Case 2- South Side at WD of 135 Degree
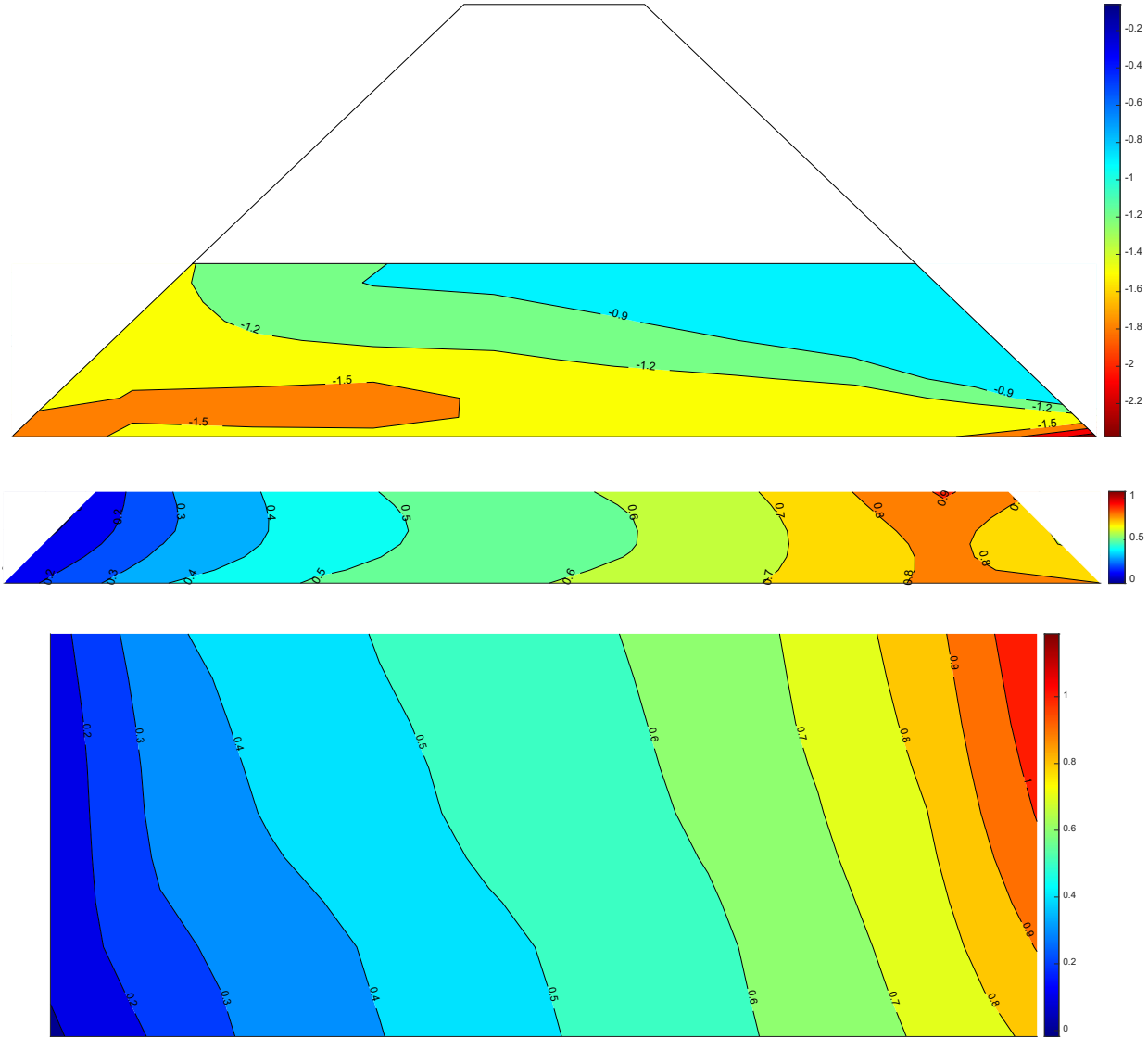
Figure 55 Peak Min Cp for roof and Peak Max Cp for wall and soffit for South Side of Model B at wind direction of 135° Open Terrain

Case 2- East Side at WD of 135 Degree
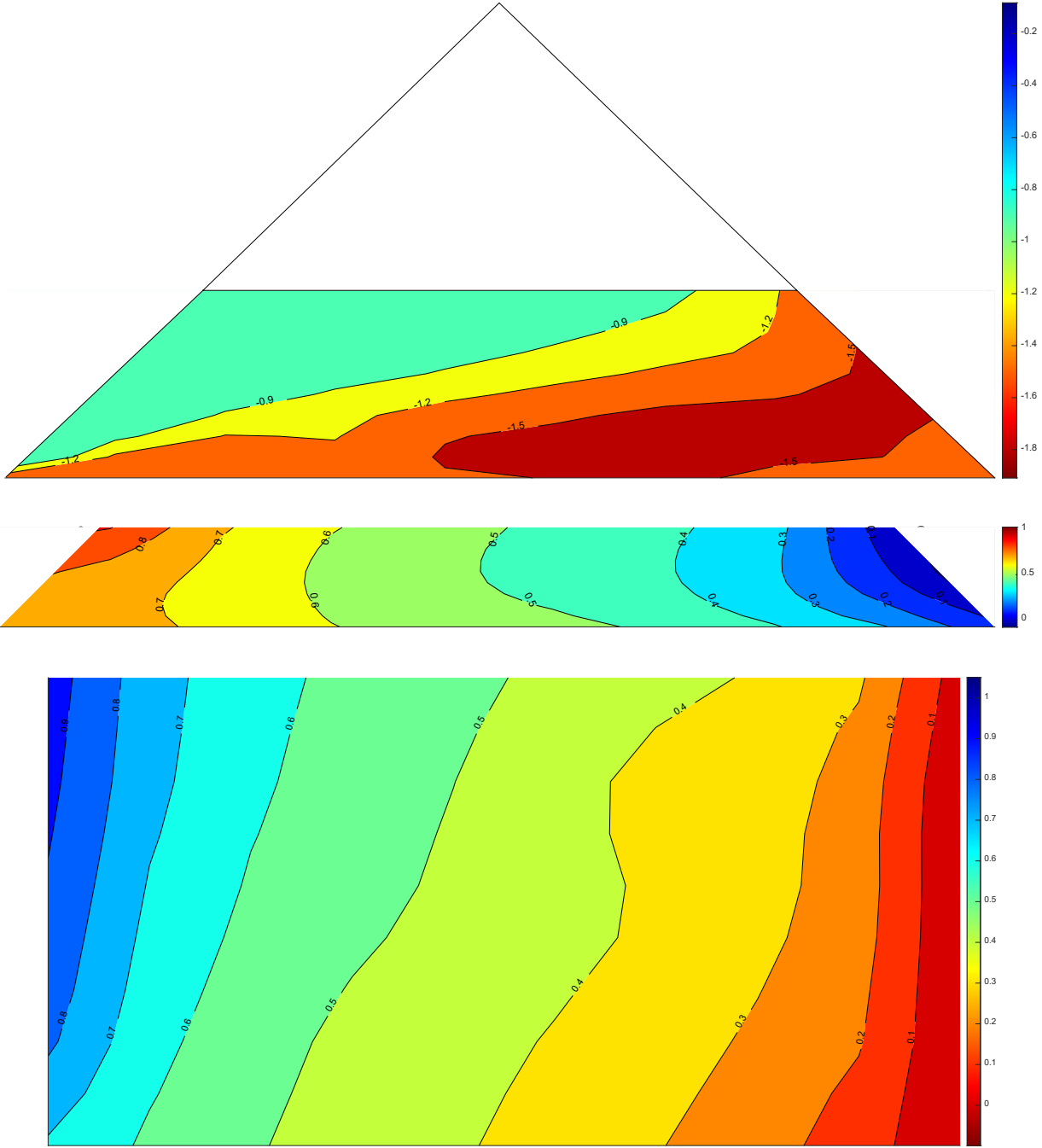
Figure 56 Peak Min Cp for roof and Peak Max Cp for wall and soffit for East Side of Model B at wind direction of 135˚ Open Terrain